TAMPEREEN TEKNILLINEN YLIOPISTO
TAMPERE UNIVERSITY OF TECHNOLOGY

Muhammad Rizwan

Design and Development of Efficient and Conformal Printed Antennas for Wireless Sensing and Wearable Applications

Julkaisu 1563 • Publication 1563

Tampere 2018

Tampereen teknillinen yliopisto. Julkaisu 1563
Tampere University of Technology. Publication 1563

Muhammad Rizwan

Design and Development of Efficient and Conformal Printed Antennas for Wireless Sensing and Wearable Applications

Thesis for the degree of Doctor of Science in Technology to be presented with due permission for public examination and criticism in Sähkötalo Building, Auditorium SA203, at Tampere University of Technology, on the 12th of October 2018, at 12 noon.

Tampereen teknillinen yliopisto - Tampere University of Technology
Tampere 2018

Doctoral candidate: Muhammad Rizwan
Wireless Identification and Sensing System (WISE)
Faculty of Biomedical Sciences and Engineering
Tampere University of Technology
Finland

Supervisor: Leena Ukkonen, Prof., Dr. Tech.
Wireless Identification and Sensing System (WISE)
Faculty of Biomedical Sciences and Engineering
Tampere University of Technology
Finland

Instructors: Lauri Sydänheimo, Prof., Dr. Tech.
Wireless Identification and Sensing System (WISE)
Faculty of Biomedical Sciences and Engineering
Tampere University of Technology
Finland

Johanna Virkki, Adj. Prof., Dr. Tech.
Wireless Identification and Sensing System (WISE)
Faculty of Biomedical Sciences and Engineering
Tampere University of Technology
Finland

Pre-examiners: Atef Z. Elsherbeni, Prof.
Department of Electrical Engineering
Colorado School of Mines
USA

Sami Barmada, Prof.
Department of Electrical Engineering
University of Pisa
Italy

Opponent: Heli Jantunen, Prof.
Faculty of Information Technology and Electrical Engineering
University of Oulu
Finland

ISBN 978-952-15-4181-0 (printed)
ISBN 978-952-15-4212-1 (PDF)
ISSN 1459-2045

Abstract

Future wireless technologies would require flexibility from electronics that will enable the electronic components to adapt according to the everyday use environment. Flexible electronics has been used in many wireless sensing and wearable applications. One of the fastest growing wireless technologies of this decade is Radio Frequency Identification (RFID) which is an automatic identification technology that uses electromagnetic interaction to identify, sense and track people or objects with transponders known as tags. RFID is rapidly replacing the bar code technology in supply chain applications and huge amount of tags are needed to be produced in order to meet the needs of this application. The production method and material selection are few of the key parameters which are under study for the cost-effective and efficient fabrication of RFID tags and wearable antennas. The latest manufacturing technologies such as inkjet, thermal and three dimensional (3D) printing have shown good potential in improving the fabrication process, however they need to be optimized and explored further to get the best possible results.

This thesis reports the use of novel manufacturing methods for the development of passive Ultra High Frequency (UHF) RFID tags and wearable antennas on versatile substrates. Commercially available as well as 3D printed flexible substrates along with different conductive inks/pastes are used for the improvement in the fabrication process. The first part of the research compares inkjet and thermal printing for the RFID fabrication in detail and suggests suitable optimizing parameters for the materials under study. The second part of the research focuses on 3D printing of the substrates and then utilizing brush painting, 3D dispensing and embroidery process to improve the overall fabrication. In addition, the fabricated antennas are tested for humidity, bending and stretching for specific applications.

The results indicate that the approach and methodologies used have great potential in improving the fabrication of RFID tags and antennas. The fabricated tags show excellent results and achieve the required performance for modern RFID applications such as supply chain, wearable biomedical sensing and environment monitoring. This detailed study will be very helpful to find out appropriate materials for fabricating wireless components with the best possible results, i.e. easy to fabricate, reliable and better wireless performance, for future applications such as Internet of Things (IoT) and smart RFID packaging.

Preface

This research work was carried out at Wireless Identification and Sensing Systems (WISE) Research Group at Department of Electronics and Communications Engineering until end of 2016, and then at BioMediTech Institute and Faculty of Biomedical Sciences and Engineering at Tampere University of Technology (TUT) during the years 2015 – 2018. The research was funded by the Academy of Finland, the Finnish Funding Agency for Technology and Innovation (TEKES) and Emil Aaltonen Foundation. The financial support is gratefully acknowledged.

I wish to thank my supervisor, Professor Leena Ukkonen, for her excellent guidance and strong support throughout my work. I also want to thank her for giving me the opportunity to complete my doctoral studies in the research group. I am also sincerely grateful to my instructors, Professor Lauri Sydänheimo and PhD Johanna Virkki, for their guidance and for their significant input to my research work. I would like to thank the collaborating team at University of Glasgow, UK, The Open University, UK and University of Montpellier, France for their contribution in Radio Frequency Identification work. I also like to thank and wish all the best to my colleagues at WISE Research Group.

Thanks to my great friends Saleem and Babar who have inspired me and have always given me strength to come this far in life. Finally and most importantly, my deepest gratitude to my parents, my family and my Fiance, Dr. Hina Kamal, for their encouragement, support and unconditional love.

Tampere, April 2018.

Muhammad Rizwan.

Contents

List of Figures

List of Tables

List of Symbols and Abbreviations

ABS	Acrylonitrile Butadiene Styrene
Ag	Silver
Al	Aluminium
AM	Additive Manufacturing
C	Centigrade
CAD	Computer Aided Design
cm	Centimeter
CTTR	Conductive Thermal Transfer Ribbons
CS	Continuous Stream
Cu	Copper
dB	Decibels
dBm	Decibel milliwatts
DC	Direct Current
DOD	Drop on Demand
DPI	Drop per Inch
DW	Direct Write
E	Electric Field
EIRP	Effective Isotropic Radiated Power
EPC	Electronic Product Code
FCC	Federal Communications Commission
FDM	Fused Deposition Modelling
GHz	Giga Hertz
H	Magnetic Field
HC	High Conductivity
HF	High Frequency
HFSS	High Frequency Structure Simulator
IC	Integrated Circuit
IoT	Internet of Things
IPL	Intense Pulsed Light
ISM	Industrial, Scientific and Medical
kHz	kilo Hertz
LF	Low Frequency
MHz	Mega Hertz
mm	Millimeter
PLA	PolyLactic Acid
RF	Radio Frequency

RFID	Radio Frequency Identification
RMS	Root Mean Square
SAR	Specific Absorption Rate
TID	Tag Identifier
UHF	Ultra High Frequency
2D	Two Dimensional
3D	Three Dimensional
Ω	Ohm
%	Percentage
µ	Micron

List of Publications

I. M. Rizwan, A. A. Kutty, M. Kgwadi, T. D. Drysdale, L. Ukkonen and J. Virkki, “Comparitive Study of Inkjet and Thermal Printing for Fabrication of Passive UHF RFID Tags,” 10th European Conference on Antennas and Propagation (EuCAP), 5 pages, Apr. 2016.

II. M. Rizwan, A. A. Kutty, M. Kgwadi, T. D. Drysdale, L. Ukkonen and J. Virkki, “Reliability study of flexible inkjet- and thermal-printed RFID antennas in high humidity conditions,” 10th European Conference on Antennas and Propagation (EuCAP), 5 pages, Apr. 2016.

III. M. Kgwadi, M. Rizwan, A. A. Kutty, J. Virkki, L. Ukkonen, T. D. Drysdale, “Performance Comparison of Inkjet and Thermal Transfer Printed Passive UHF RFID Tags,” IET Microwaves, Antennas & Propagation, vol. 10, no. 14, pp. 1507-1514, Nov. 2016.

IV. M. Rizwan, A. A. Kutty, M. Kgwadi, T. D. Drysdale, L Sydänheimo, L. Ukkonen and J. Virkki, “Possibilities of Fabricating Copper-based RFID Tags with Photonic-sintered Inkjet Printing and Thermal Transfer Printing,” IEEE Antennas and Wireless Propagation Letters, vol. no. 16, pp. 1828-1831, Mar. 2017.

V. M. Rizwan, M. W. A. Khan, L. Sydänheimo, J. Virkki, and L. Ukkonen, “Flexible and Stretchable Brush-Painted Wearable Antenna on a 3D Printed Substrate,” IEEE Antennas and Wireless Propagation Letters, vol. 16, pp. 3108-3112, Oct. 2017.

VI. M. Rizwan, M. W. A. Khan, H. He, J. Virkki, L. Sydänheimo and L. Ukkonen, “Flexible and stretchable 3D printed passive UHF RFID tag,” IET Electronics Letters, vol. 53, no. 15, pp. 1054-1056, Jul. 2017.

VII. M. Rizwan, M. Guibert, A. Massicart, J. Torres, L. Sydänheimo, L. Ukkonen, T. Björninen and J. Virkki, “Embroidered Passive UHF RFID Tag on Flexible 3D Printed Substrate,” Progress in Electromagnetics Research Symposium, pp. 818-822, Feb. 2018.

1 Introduction

The Internet of Things (IoT) has enabled physical objects to communicate and identify with other objects as well as the environment. These physical objects can be termed as smart devices and contain electronics as an integral part. Most of these electronics are embedded and flexible electronics which is needed in abundance for the current wireless applications and ubiquitous sensing networks. The manufacturing of these electronics has a huge impact on the overall efficiency of the system. Radio Frequency Identification (RFID) technology is an essential enabling building block for IoT [1-3].

The RFID technology can identify and track items with low cost battery free electronic tags [4-6]. The tag consists of an antenna and Integrated Circuit (IC). The system uses electromagnetic waves in different frequency bands for powering up and then communicating with these passive tags. It offers the benefit of rapidly interrogating large numbers of tags through various dielectric media such as paper, cardboard and plastic. Due to their modulated backscattering principle, the information stored inside the tag's IC can be read from several meters. Previously, RFID was utilized in applications such as tracking (Intelligent steel inventory tracking, real time locating and retail [7-9]), access control (Border control system [10]), food quality control [11] but now it is used in traffic management [12], environment monitoring (Temperature or gas sensors [13-15]) and healthcare (noninvasive wearable and wireless on-skin sensing [16-18]). Due to its deployment on a large scale, industries are taking interest in improving the manufacturing of smart products such as passive Ultra High Frequency (UHF) RFID tags and compact wearable sensors by using the latest manufacturing technologies.

Additive Manufacturing (AM) methods have shown huge potential in improving the manufacturing of RF components [19-20]. The main advantage of these methods is that they can be applied to wide range of substrates such as paper, wood and plastic. The cost of the whole RFID system can be reduced if low cost substrate and conductive material is used. The manufacturing methods with high future potential are inkjet printing [21-25], thermal printing [26] and three dimensional (3D) printing [27-32]. The main challenge involved in manufacturing is that these methods need to be optimized

for every substrate and conductive material. Also, all of these fabrication methods have some restrictions and shortcomings, and thus finding the most suitable fabrication method for each application and substrate can be challenging. The key points with respect to methods mentioned above are :

1. For inkjet printing, the compatibility of the different substrates with available low cost conductive materials such as copper. The final printed sample should be successfully sintered using the post-processing methods such as heat sintering and photonic sintering. Heat sintering is a slow method while photonic sintering is fast and can transfer more energy to quickly reduce low cost materials such as copper that require high temperature for reduction. This can damage the substrate and limits the use of different substrates for inkjet printing [25]. New substrates should be explored to further analyze this challenge of sintering low cost material using the inkjet printer.
2. Thermal printing is a quick and an easy method for printing and has shown good potential for printing RF components [26]. This printing method can be good alternate to inkjet printing but is not explored for RFID tag manufacturing.
3. 3D printing is the latest method which is used for the manufacturing of RFID tags and antennas, however the traditional materials used are non-flexible [27-29], making it less suitable for emerging wireless technologies specially in flexible electronics and body worn applications. Another issue with current 3D printed tags and antennas is that the conductive material is rigid and unreliable [27-29, 31].

These key points need to be addressed to improve the overall manufacturing and the performance of the RFID tags and antennas to adopt the future wireless technologies such as IoT. Keeping in view the above points and to ease the manufacturing challenges for future researchers, it is necessary to study all these manufacturing technologies and help understand the suitable methods in different fabrication cases for RFID and wearable antennas.

1.1 Objectives and scope of the thesis

The work presented is focused on studying the novel manufacturing methods for the development of passive UHF RFID tags and wearable antennas on versatile substrates. The objective of the thesis is to solve the challenges listed, which is achieved in the following ways:

1. Fabrication of inkjet and thermal printed passive UHF RFID tags on novel paper/polyester based substrate (Flexcon THERMLfilm).
   i) Optimizing the printing parameters for the novel substrate for both the printing methods.
   ii) The reliability study of fabricated tags and their performance comparison.
   iii) Exploring the possibility of utilizing low cost conductive materials for printing the tags.

2. Development of flexible 3D printed passive UHF RFID tags and wearable antennas.
   i) Flexible 3D printed substrate and its characterisation.
   ii) Replacing the non-flexible conductor with flexible conductor.
   iii) Combining the manufacturing methods to produce more reliable RFID tags.

Inkjet printing, thermal printing, 3D dispensing and 3D printing are used to print Silver (Ag), Aluminium (Al) and Copper (Cu) based inks/conductor/paste on substrates like polyimide (Kapton), paper/polyester (Flexcon THERMLfilm) and NinjaFlex. Kapton and THERMLfilm substrates are commercially available however, NinjaFlex is 3D printed to be used as substrate. One of the key part of the thesis is printing flexible substrate using 3D printing and characterizing it with different thickness on UHF band. This 3D printing method is then combined with other methods (Brush painting, 3D dispensing and embroidery) to produce hybrid manufacturing. In each of the study, optimization of printing parameters and post-processing (thermal and photonic) is completed extensively. The performance of the manufactured RFID tags and antennas is evaluated through wireless measurements. The measurements are supported by simulations carried out in High Frequency Structure Simulator (HFSS) v.16. Material characterisation of 3D printed NinjaFlex is also carried out for simulations using Agilent 85070E dielectric probe kit. The read ranges of the fabricated tags changed depending on the substrates as well as the conductive material used. For inkjet printing, Harima NPS-JL Ag [33] and ANI Cu-IJ70 Cu nano-particle [34] inks are used while, for 3D dispensing DuPont PE872 stretchable Ag conductive paste [35] is used. Apart from printing, few quick methods like brush painting and embroidery are also used.

The scope of this thesis is to optimize the available manufacturing methods for achieving excellent RF performance for passive UHF RFID tags and wearable antennas with versatile substrates. Following steps are taken to fulfil the scope of the thesis: Comparison of inkjet and thermal printing for polyimide (Kapton) and paper/polyester (Flexcon THERMLfilm) substrate using Ag and Al conductor (Publication I), and their reliability study (Publication II). Adopting Cu metal and exploring photonic sintering in the inkjet printing (Publications III and IV). The fabrication, performance and bending analysis of a flexible and stretchable wearable antenna on a NinjaFlex substrate using brush painting (Publication V). Exploring the possibility of dispensing stretchable Ag conductive paste on NinjaFlex substrate for UHF RFID tags manufacturing (Publication VI). Replacing the dispensing stretchable Ag conductive paste and embroidering Ag plated thread on 3D printed NinjaFlex substrate (Publication VII).

1.2 Structure of the thesis

The structure of this thesis is divided into six chapters. Chapter 1 introduces to the objectives and scope of the thesis along with the thesis division and author's contribution in the publications. Chapter 2 includes the basic introduction to RFID technologies, how it works, the important aspects of

RFID (Tag specifications and IC) and measurements tools. Chapter 3 describes the antenna fabrication methods used in this study. Details of the manufacturing process, equipment and materials required are also explained in this chapter. Chapter 4 is related to inkjet and thermal printing for passive UHF RFID tags on novel substrates. Chapter 5 discusses the 3D printing for the manufacturing of wearable antennas and passive UHF RFID tags on NinjaFlex substrate. Chapter 6 concludes the work presented in this thesis and presents the new research directions opened by this thesis work.

1.3 Author's contribution

This thesis consists of seven publications. Chapter 4 and 5 discusses the methods and results presented in these publications. The author's contributions are as follows:

Publication I: The author is the main contributor of the publication. The publication is about the comparison of inkjet and thermal printing for the fabrication of passive UHF RFID tags. The inkjet printing is done by the author along with Ajith Adhur Kutty and the thermal printing is done by Monageng Kgwadi in University of Glasgow, United Kingdom. The inkjet printing work, the measurements of all the samples including thermal printed samples and the analysis on the results has been done by the author. The author also wrote the manuscript and the co-authors reviewed, commented and improved the text.

Publication II: The author is the main contributor of the publication. The publication is about the reliability study of passive UHF RFID tags fabricated in Publication I. The reliability tests, the measurements of all the samples including thermal printed samples and the analysis on the results has been done by the author. The author also wrote the manuscript and the co-authors reviewed, commented and improved the text.

Publication III: The publication extends the work done in Publication II. The author contributed in the inkjet printing, the measurements of all the samples and the analysis on the results. The manuscript is written in co-operation with Monageng Kgwadi and the co-authors reviewed, commented and improved the text.

Publication IV: The author is the main contributor of the publication which extends the work done in Publication III. The publication explored the possibilities of manufacturing Cu based passive UHF RFID tags using inkjet and thermal printing on two substrate materials, polyimide (Kapton) and a polyester based substrate (Flexcon THERMLfilm). The inkjet printing work, its post-processing, the measurements of all the samples including thermal printed samples and the analysis of the results has been done by the author. The author also wrote the manuscript and the co-authors reviewed, commented and improved the text.

Publication V: The author is the main contributor of the publication. The publication is about the proof-of-concept of the fabrication and performance analysis of a flexible and stretchable wearable antenna on a 3D printed substrate. The author did the 3D printing of substrate. Brush painting and RF measurements are done with the help of M. Waqas A. Khan. The author wrote the manuscript and the co-authors reviewed, commented and improved the text.

Publication VI: The author is the main contributor of the publication. The publication presents the fabrication and analysis of a flexible and stretchable 3D printed passive UHF RFID tag. The author did the 3D printing of substrate. The 3D dispensing is done by Han He. The author and M. Waqas A. Khan carried out the characterisation of the 3D printed substrate, planned and performed the stretching test and analyzed the wireless measurements of the fabricated tags. The author wrote the manuscript and the co-authors reviewed, commented and improved the text.

Publication VII: The author is the main contributor of the publication. The publication presents fabrication and wireless evaluation of embroidered passive UHF RFID tags on a 3D printed substrate. The author primarily planned this paper and carried out all fabrication steps along with Maxime Guibert and Alexandre Massicart from University of Montpellier, France. The author carried out the characterisation of the 3D printed substrate and analyzed the wireless measurements of the embroidered tags. The author wrote the manuscript and the co-authors reviewed, commented and improved the text.

2 Radio frequency identification technology

RFID is a wireless automatic identification technology that uses electromagnetic interaction to identify, sense and track people or objects with transponders i.e. tags [5]. The advantage this technology offers over its predecessors (bar code reading) in identification is non-line of sight wireless detection. Figure. 1 shows a basic RFID system. The system has three main parts: reader device, reader antenna and tag. The whole system can be attached to a computer/server with an application that can convert the data into human readable format. The RFID tag consists of a tag antenna and IC. The IC stores the data in the memory and uses impedance modulation to establish communication between the reader and the tag. Typically, the IC has a specific wake up power which should be received at the tag antenna so that the IC starts working. The performance of an RFID tag is normally described by its read range i.e. the maximum distance between the reader and the tag at which the tag can communicate and still be read with the reader [36,37].

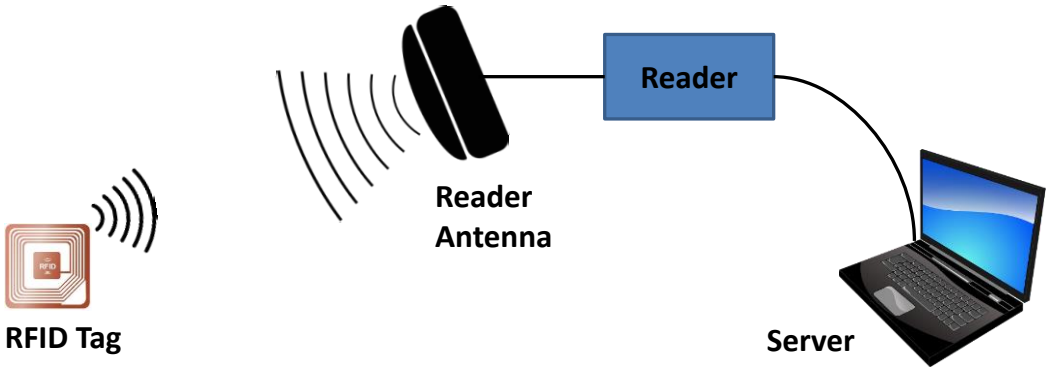

Figure 1: RFID system.

2.1 Classification of RFID tags

The RFID tags can be classified based on three different categories [36-38]:

2.1.1 Based on frequency of operation

The RFID tags can be classified in three different frequency ranges based on their frequency of operation:

Low Frequency (LF)

The LF tags operate in the range of 125 kHz-134 kHz. The read range of these types of tag is usually few centimetres (cm).

High Frequency (HF)

The HF tags operate at 13.56 MHz central frequency. The read range of these types of tag is usually few centimetres to few meters (around 1 m).

Ultra High Frequency (UHF)

The UHF tags operate in the range of 806 MHz-960 MHz and at 2.4 GHz central frequency. The read range of these types of tag is usually few meters up to hundreds of meters.

Figure. 2 shows commercially available RFID tags.

Figure 2: Commercially available RFID tags, LF (Top), HF (Middle) and UHF (Bottom).

2.1.2 Based on electromagnetic interaction

The RFID tags can be categorised into two types based on the electromagnetic interaction; Near-field and far-field. The LF and HF RFID tags use near-field coupling while the UHF RFID tags use far-field for communication. The near-field RFID tags have smaller read range due to the rapid decaying of energy however the far-field RFID tags have larger read ranges and smaller size.

2.1.3 Based on power supply for the tag

The RFID tags can be classified in three different categories based on the power supply of the tag:

Active RFID tags

The active RFID tags have their own power supply and do not rely on power supplied by the reader antenna for communication. These types of RFID tags have large read ranges but the life span of systems depends on the life span of the power source. The cost of active RFID is also higher in comparison with other types due to the presence of the power supply.

Semi-passive RFID tags

The semi-passive RFID tags have a power supply to activate the IC but use reader antenna's power for communication. The read range of these tags is less than the active RFID tags.

Passive RFID tags

The passive RFID tags have no power supply and completely rely on the reader antenna's power for activating the IC as well as for data transmission. Passive RFID tags have a long life span and do not need any maintenance or battery replacement. Due to this, passive RFID tags have low cost and are abundantly used in the wireless sensing applications nowadays.

Table.1 summarizes the classification of RFID tags, their general properties and applications.

Table 1: Classification of RFID tags and their general properties [36-38]

Frequency range	Typical read ranges	Electromagnetic interaction	General characteristics	Applications
LF 125 kHz-134 kHz	Few cms to 2 m	Near-Field	Affected by electrical noise Low data rate Shorter read range	Access control Animal tagging
HF 13.56 MHz	Approx. 1 m	Near-Field	Prone to electrical noise Better data rate than in LF Better read range than in LF	Logistics Supply chain Credit cards

UHF 806 MHz-960 MHz and 2.4 GHz	Few meters to hundred meters Typically 5 m	Far-Field	Smaller size Low cost Larger read range High data rate	Supply chain Parking access control Electronic toll collection

The focus of this thesis is on the passive UHF RFID due to its advantages such as smaller size, low cost, longer life span and larger read range distance.

2.2 Fundamental parameters of antennas

The antenna is the most essential component of a communication system. According to Webster's Dictionary, an antenna is defined as: "It is usually a metallic device (as a rod or wire) for transmitting or receiving waves". Antennas are passive components and are reciprocal devices i.e. its properties remain the same whether it is used as a receiving or a transmitting device. Time-varying current or an acceleration (or deceleration) of charges are two conditions that need to be met to produce time varying E (Electric) and H (Magnetic) fields in the antenna. When these two conditions are met, the antenna will radiate in all directions [39,40].

2.2.1 Radiation fields near an antenna

The radiation field near an antenna can be separated into three regions that are reactive near-field, radiating near-field (Fresnel Zone) and far field (Fraunhofer Zone) [39]. The reactive near-field is immediately near to the antenna where the reactive fields predominates. Generally, the reactive near-field of the antenna is at a distance $R < 0.62\sqrt{\frac{D^3}{\lambda}}$ from the antenna surface, where λ is the wave-length and D is the largest dimension of the antenna. The radiating near-field or the Fresnel zone lies in between the reactive near-field and the far-field region. In this field the angular field distribution is dependent upon the distance from the antenna. The radiating near-field lies at a distance range of $0.62\sqrt{\frac{D^3}{\lambda}} < R < \frac{2D^2}{\lambda}$. As explained in the classification of RFID tags, the LF and the HF tags operate in near-field region and due to the rapid decaying of fields, the read range of these tags are limited. The most important field region is the far-field region where the radiation pattern does not change shape with distance and a propagating wave can be assumed as a plane wave. The far-field region start from $R > \frac{2D^2}{\lambda}$ and expands away from the antenna.

2.2.2 Radiation pattern

The graphical representation of the field strength transmitted or received by the antenna is known as radiation pattern [39]. The radiation pattern can be divided into two planes i.e. E-plane and H-plane. Both these planes have their corresponding E-plane and H-plane vectors. The radiation pattern is usually defined in the far-field region of the antenna because the field distribution is independent of the distance from the antenna. Based on the pattern of radiation we can classify antennas into three types: isotropic, omni-directional and directional radiation patterns. An isotropic antenna radiate fields equally in all directions. This type of radiator is considered the ideal case. The omni-directional antenna radiate fields in a specific plane however, a directional antenna radiate fields in a specific direction. The radiation pattern is generally described in decibels (dB) scales.

2.2.3 Directivity, efficiency and gain

The directivity of an antenna is the ration of radiation intensity in a specific direction to the average radiation intensity (Eq. 1). The radiation intensity $U(\theta,\phi)$ is the power radiated in a given direction per unit solid angle, measured in watts per steradians or square radians [41].

$$D\ (\theta,\phi) = \frac{U\ (\theta,\phi)}{U_{av}} = \frac{U\ (\theta,\phi)}{\frac{1}{4\pi}\int_0^{2\pi}\int_0^{\pi} U\ (\theta,\phi)\ sin\theta\ d\theta\ d\phi}\ . \tag{1}$$

The antenna directivity is a dimension less quantity and its value ranges from unity (for isotropic antenna) to greater than unity (for non-isotropic antennas). The directivity is generally expressed in dBi i.e. the directivity of the antenna under test over the directivity of an isotropic antenna.

The efficiency of the antenna, considered to be loss less (Input power is equal to radiated power), is 1, however practically this is not possible. Some of the power is lost in ohmic and other losses i.e. P_{ohmic}. The efficiency of the antenna can be expressed as Eq. 2 [41]:

$$e_{cd}\ = \frac{P_{rad}}{P_{in}} = \frac{P_{rad}}{P_{rad} + P_{ohmic}}\ . \tag{2}$$

Another important loss is due to the mismatch between the antenna input terminals and the antenna feed line. This is known as reflection or mismatch efficiency e_r. Hence, the total efficiency of the antenna can be expressed as,

$$e_{total} = e_{cd}\ e_r\ . \tag{3}$$

Gain or power gain shows how efficiently the available power at the input terminals of the antenna is transmitted. The unit of gain is dB; if taken considering the isotropic antenna then it is represented in dBi. Gain and directivity are related to each other by the efficiency of the antenna as [39] [41],

$$G = e_{total}\ D\ (\theta,\phi)\ . \tag{4}$$

2.2.4 Input impedance

The input impedance is the impedance at the input terminals of an antenna which is written as:

$$Z_A = R_A + jX_A \ . \tag{5}$$

where, real part of the impedance represents power that is either radiated away or absorbed within the antenna while the imaginary part represents the power that is stored in the near field of the antenna. The real part R_A is a combination of radiation resistance R_r and loss resistance R_L. The radiation resistance R_r represents the radiated power and loss resistance R_L represents the power dissipated as heat [39] [41].

2.3 Performance metrics in passive UHF RFID tags

2.3.1 Impedance matching

To have an efficient power transfer between the IC and RFID tag antenna, a proper impedance matching needs to be assured. Figure. 3 shows the equivalent circuit model of a passive RFID tag with IC.

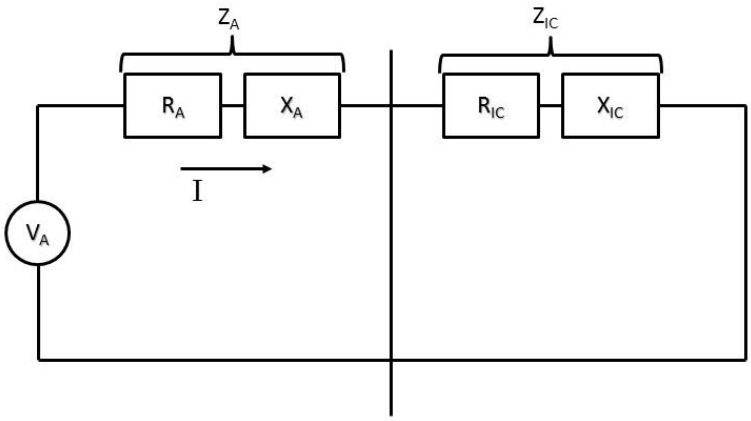

Figure 3: Equivalent circuit of passive RFID tag.

The circuit shows two complex impedances Z_A and Z_{IC} which should be matched in order to transfer maximum power and enable the best possible operation. From the circuit, current and power reflection coefficient can be express as,

$$I = \frac{V_A}{Z_A + Z_{IC}} \ . \tag{6}$$

$$\Gamma = \frac{Z_{IC} - Z_A^*}{Z_{IC} + Z_A} \ . \tag{7}$$

Γ is the power reflection coefficient which represents the mismatch between the antenna and the IC impedances [42]. An alternate way is to express it as the power transmission coefficient [43].

$$\tau = 1 - |\Gamma|^2 \text{ where } 0 \leq \tau \leq 1. \quad (8)$$

The tag IC has nonlinear input power and frequency dependent input impedance which is capacitive thus to have a perfect matching and maximum power transfer, the input reactance of the tag antenna input impedance should be inductive [44]. In reality, commonly used tag antennas such as small dipoles have capacitive input reactance [39]. This implies a need for transforming the input impedance of the antenna to inductive. This is achieved by using a matching network between the IC and the RFID tag antenna [45,46].

2.3.2 Read range

The maximum distance at which the information stored in the RFID tag IC can successfully be read by the reader is known as the read range [5]. It is the most important performance indicator of an RFID tag. Usually from an RFID tag designer perspective, the impedance matching, the IC wake up power and the realized gain are the three important factors that can increase the read range.

2.3.3 Threshold power

The transmission power required to wake up the IC is known as threshold power [5]. A low threshold power will allow longer read ranges. The threshold power of a tag can be expressed using the Friis transmission equation:

$$P_{TS} = \frac{P_{IC}}{G_{tx}G_{tag}\tau\left(\frac{\lambda}{4\pi d}\right)^2 |\hat{p}_{tx}\cdot\hat{p}_{tag}|^2} \ . \quad (9)$$

where P_{IC} is the wake up power of the IC, G_{tx} and G_{tag} are the gains of reader antenna and tag antenna. λ is the wavelength, τ is the power transmission coefficient. d is the distance between the reader and the tag. $\hat{p}_{tx}$ and $\hat{p}_{tag}$ are the unit electric field vectors of both the antennas.

The system will work when the power received on tag (P_{tag}) will be equal to the wake up power of the IC (P_{IC}). The equation can be written as [39] [47,48],

$$P_{tag} = P_{tx}G_{tx}G_{tag}\left(\frac{\lambda}{4\pi d}\right)^2 \ . \quad (10)$$

where P_{tag} is the power received on the tag and P_{tx} is the power transmitted by the reader antenna. This implies that the theoretical read range to be:

$$d_{tag} = \frac{\lambda}{4\pi}\sqrt{\frac{P_{tx}G_{tx}G_{tag}\tau}{P_{TS}}} \ . \quad (11)$$

2.4 Integrated circuit

An RFID tag has two main parts: a tag antenna and an IC. The IC contains a memory unit which stores the information. This memory is read and write both and can be used to identify a specific object on which the RFID tag is placed. In this study NXP UCODE G2iL series IC is used [49]. The chip has a wake up power of 15.8 µW (-18 dBm), 128 bit Electronic Product Code (EPC) memory and 64-bit Tag IDentifier (TID) including 32-bit factory locked unique serial number. Figure. 4 shows the NXP UCODE G2iL series IC. As seen in Figure. 4 the IC has 2 3x3 mm^2 pads for attachment. The IC has an equivalent input parallel resistance and capacitance of 2.85 kΩ and 0.91 pF respectively [50]. In this study, we used Circuit Works conductive Ag epoxy CW2400 to attach the IC to the RFID tags. The attachment is done by hand and after the attachment, the interconnection is sintered for 10 minutes at 70 °C in the oven. If an oven is not available then the interconnection is left for four hours to dry at room temperature.

Figure 4: NXP UCODE G2iL series IC used in the RFID study.

2.5 RFID measurement system

In this study, Voyantic Tagformance lite UHF RFID measurements system is used for the wireless measurements of the fabricated tags, shown in Figure. 5. The system has a small anechoic chamber (120 × 80 × 80 cm^3), as shown in Figure. 6, in which the tag can be placed for the measurements. The antenna of the RFID reader is linearly polarised patch antenna with the gain of 8 dB and operates between 800-1000 MHz. The output of reader ranges from 0 to 27 decibel milliwatts (dBm) and the Radio Frequency (RF) receiver has sensitivity of -75 dBm.

Figure 5: Voyantic Tagformance lite.

Figure 6: Inside the Voyantic measurement unit.

The system uses the measured threshold power and the measured forward losses for calculating the theoretical read range of a tag [51]. The system is first calibrated using a reference tag which calculates the forward losses. The calibration is the most important step in which the reference tag should be placed at the same location inside anechoic chamber which the tag under study would be placed afterward for the measurements. The system calculates the power required to activate the reference tag and then calculates the path loss which includes polarization losses, cable losses, reader antenna gain and losses. Apart from threshold power measurements, the system can also measure the radiation pattern of the tags at a certain frequency.

When comparing the Tagformance measurement system with the earlier theory explain in section 2.3.3 and in equation 9-11, the system measures the threshold power P_{TS} by increasing the transmitted power until the tag responds to the query made by the reader. This is effected by the wake up power of the IC. The forward loss from the transmit port to the tag is calculated using a reference tag during the calibration of the Tagformance measurement system. The theoretical read range measured is thus limited by the maximal allowed transmitted power and can be calculated as:

$$d_{tag} = \frac{\lambda}{4\pi}\sqrt{\frac{EIRP}{P_{TS}L_{fwd}}} \quad . \tag{12}$$

where λ is the wavelength, *EIRP* is the effective isotropic radiated power which is the maximum isotropic radiated power allowed by the regulations i.e. 3.28 W in Europe and 4 W in US. *EIRP* can be expressed as a product of transmitted power P_{tx} and the gain of the transmitting antenna G_{tx}. L_{fwd} is the quantity which represents measured forward losses.

In this study, the Tagformance measurement system is used for the theoretical read range measurement after the fabrication of the tags and is referred to as measured theoretical read range to differentiate it from the simulated theoretical read range. Also, it is called measured theoretical read range because it is not actually measured but calculated based on threshold power of the tag and the reference tag that are actually measured.

3 Antenna manufacturing methods

This chapter explains different manufacturing methods for the fabrication of the antenna including both the conductive trace and the substrate part. For the conductive part, the methods used are inkjet printing, thermal printing, 3D dispensing and brush painting, whereas, for the substrate part, 3D printing is used. Post-processing methods are also explained at the end of the chapter along with the antenna designs that are used in Publications I-VII.

3.1 Additive manufacturing

AM is a process in which a material is deposited layer-by-layer to make a design. In particular to the manufacturing of the antennas, this technology is used to either deposit the conductive material on the substrates or to make new substrates [52]. The AM technology is also termed as Rapid Prototyping. The process is quick, accurate and wastes less amount of material (mostly conductive material) which makes it more suitable for the manufacturing of the antennas where conductive materials are expensive. Nearly all of the AM machines have a software that can be used to optimize the design and have an accuracy level of micro meters. The machines can deposit a wide range of materials including nano-particle conductive inks, screen printable inks and plastics. At the end of the AM process, the deposited material might require a post-processing.

3.1.1 Direct write (DW) technologies

The direct write technologies can create two dimensional (2D) and 3D structures on flat, flexible or conformal surfaces in simple or complex geometry. Instead of using a mask for making the structure, the DW has a computer generated design file which the software of the machine can optimize and print accordingly [52-54]. The main application of DW includes printable electronics such as printing antennas, passive components and batteries. DW has five categories: ink-based, thermal spray, laser-transfer, beam deposition, liquid-phase, and beam tracing processes [52].

Ink-based DW technology

The ink-based DW is widely used in manufacturing due to its simplicity and cost-effectiveness. The inks, containing the desired material, are deposited on the surface using a machine. These inks are composed of the solvent and a certain percentage of desired material. After deposition, post-processing is carried out to convert the ink into material having desirable properties e.g. high conductivity. Out of all the ink types, nano-particle inks are the most used nowadays. Ink-based DW can be done by either depositing ink in drops with a print head or extruding continuously as a filament [52,53]. Figure. 7 shows both the deposition methods.

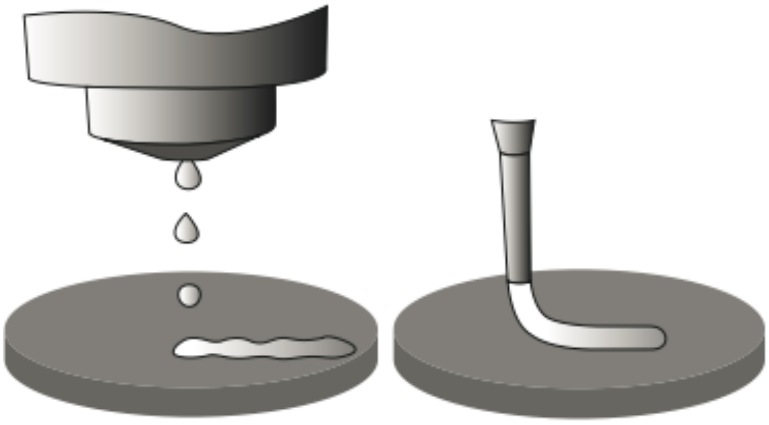

(a) (b)

Figure 7: Inkjet based direct writing techniques: (a) Jetting droplets (b) Continuous flow [52].

3.1.1.1 Inkjet printing

Inkjet printing has been used to manufacture antennas on versatile substrates such as paper, wood and cardboards. The main advantage is highly accurate printing with a wide range of print resolution. It is a contactless printing method i.e. the print head does not come into contact with the substrate on which it is printing [55]. Each printer consists of a computer aided software which can make as well as optimize a design. The inkjet printers are capable of depositing ink in drops (Drop on Demand) or Continuously Stream (CS) through a print head. The CS is a simple process however the DOD is complex and more effective. The printers capable of DOD mode utilize a pressure pulse or jetting pulse for the drop formation [52]. The shape and size of drops depend on the jetting pulse shape. The actuator is responsible for forming these pulses. Figure. 8 shows the drop formation in DOD inkjet printers.

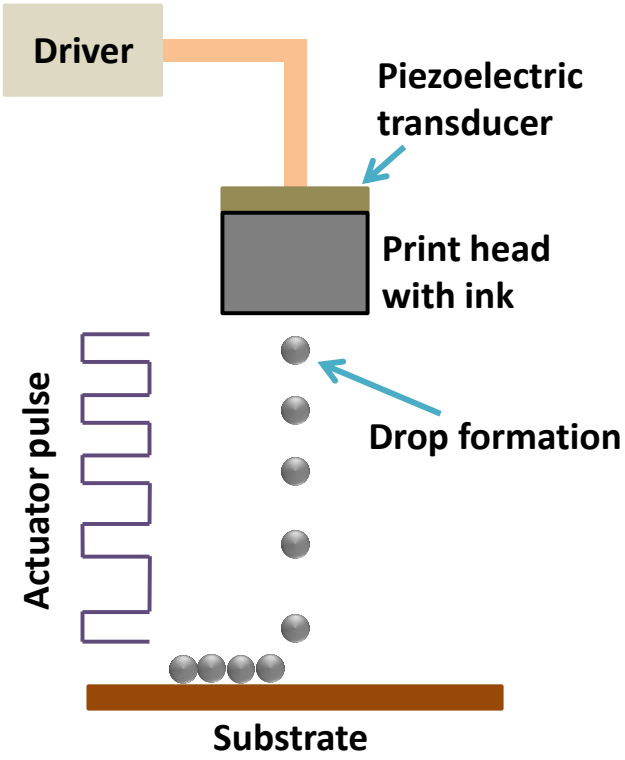

Figure 8: Illustration of Inkjet printing with drop on demand principle.

The inkjet printer used in this study is Fujifilm Dimatix DMP-2831 material inkjet printer shown in Figure. 9. The printer has a print carriage which moves according to the design and holds the ink cartridge. The drop watcher is used to see the formation of drops and how they will be dropped on the substrate. The substrate is placed on the platen of the inkjet printer. The printer is a DOD inkjet printer and the ink cartridge has 16 nozzles each having 10 picoliter (pl) drop volume capacity. As the printer works on DOD principle, the final goal is to have a good print quality of the design.

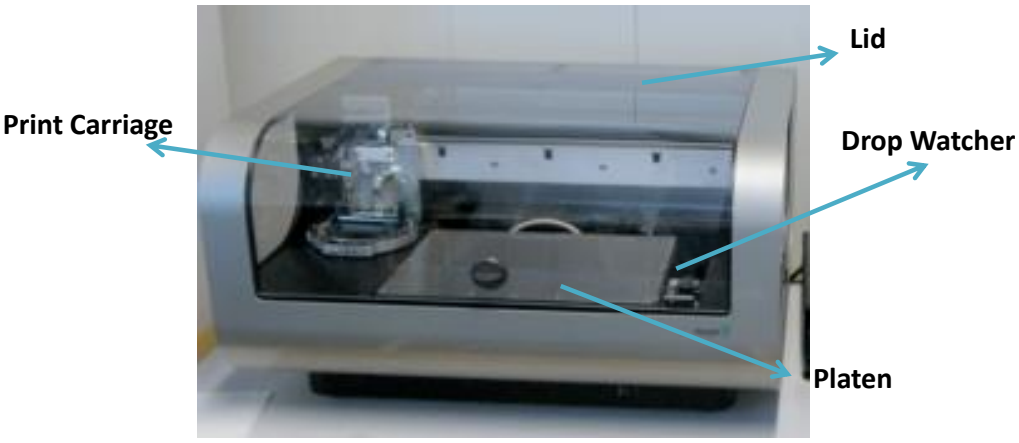

Figure 9: Fujifilm Dimatix DMP-2831 inkjet printer.

The print quality is effected by several parameters which include jetting pulse shape, the temperature of the platen and the ink cartridge, the number of nozzles used and the pattern resolution [52] [55].

Jetting pulse shape

Drop formation is the most important part of the printing process in inkjet printing. The jetting pulse shape or waveform determines the drop formation. A voltage pulse is applied to the piezo-electric transducer for each drop that ejects from the nozzle of the printer. A typical jetting pulse waveform can be seen in Figure. 10.

Figure 10: Jetting pulse waveform of inkjet printer.

The pulse width and the amplitude have effects on the drop velocity. For a particular pulse width, the increase in pulse voltage increases the drop velocity which means that increase in pulse voltage will increase the drop formation and hence more ink will drop in the width. The jetting frequency also has similar effect where the increase in frequency increases the drop velocity and size of the drop. The jetting voltage ranges from 0-40 Volts (V).

Temperature of the platen and the ink cartridge

The temperature of the platen and ink have huge impact on the final print quality. The platen temperature can be adjusted up to 60 °C. It determines how quickly the ink drop dries on the substrate. The ink cartridge temperature effects the flow of the ink and varies from 28 to 70 °C. A higher temperature will allow the ink to flow more and thus a low pulse voltage will be required for the drop formation.

Number of nozzles

The Fujifilm Dimatix DMP-2831 print head of the ink cartridge have 16 nozzles. Before starting the printing, the user can select the number of nozzles and the particular number of nozzle to be used for printing. Increasing the number of nozzles decreases the time taken to complete a print.

Pattern resolution

The pattern resolution or print resolution is determined by the drop spacing. The drop spacing is the distance between two drops from center to center. For example, if the drop spacing is 50 microns then the distance between two adjacent drops in X-axis and Y-axis will be 50 microns apart from the center. The cartridge mounting angle plays an important role in getting the same resolution in both directions. The pattern resolution varies from 100 DPI (Drops per inches) to 5080 DPI.

The inkjet printable inks have low viscosity so that they can easily flow and the drop formation process can be efficient. Although with benefits such as high accuracy and more control on lots of printing parameters, the inkjet printing is a slow printing method and the amount of ink coming out of the nozzle makes a very thin layer on the substrate. The speed of printing can be increased to some extend by optimizing the jetting waveform or by using multiple nozzles at the same time while the thin layer can be increased by depositing multiple layers instead of single to have a thick pattern on the substrate [56,57].

3.1.1.2 3D dispensing

3D dispensing is a type of continuous nozzle dispensing process [58,59]. A smart pump is used to push the ink towards the nozzle. The size of nozzle determines the amount of ink as well as the accuracy of the pattern. The 3D dispensing does not require a mask and have a computer aided software for optimizing the design. NScrypt tabletop series 3D direct write dispensing system shown in Figure. 11 is used in this study for the antenna manufacturing.

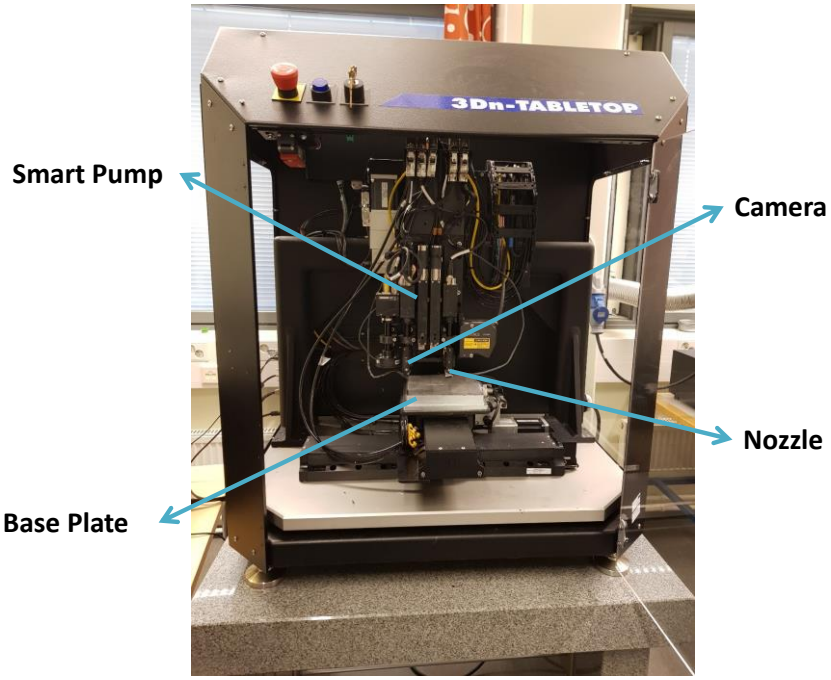

Figure 11: NScrypt tabletop series 3D direct write dispensing system.

The system is highly accurate and can import designs from many Computer Aided Design (CAD) tools. Screen printed inks are mostly used for the manufacturing of the antenna using the dispenser [58]. Post-processing is done after the dispensing method in order to convert the inks into conductive form. The print quality is effected by several parameters which include the speed of printing, the nozzle size, the dispensing gap, the opening and closing of the valve [60].

Speed of printing

The printing speed determines how quickly the design can be dispensed however it needs to be matched with the opening and the closing of the nozzle to properly dispense the ink on the desired area. The maximum printing speed the nScrypt tabletop series 3D direct write dispensing system can offer is 300 mm/s.

Nozzle size

The dispensing system has variety of nozzle sizes ranging from 12.5 to 125 micrometer (µm). The tips are highly fragile and can break very easily. Figure. 12 shows a typical nozzle for the dispensing system.

Figure 12: Typical nozzle of Nscrypt 3D dispensing system.

Dispensing gap

The dispensing gap is the distance between the substrate surface and the nozzle tip. Figure. 13 illustrates how the ink is deposited on a substrate from pump “p”. If the gap is not set properly then the ink can gather at some points to make the pattern non-uniform, also if the tip is too close to the substrate then printing multiple layers can affect the final design.

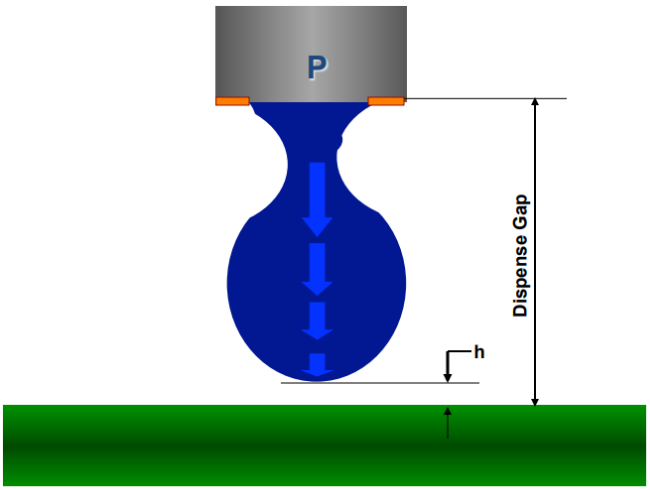

Figure 13: Illustration of dispensing gap between nozzle and substrate.

Opening and closing of valve

Opening and closing of the valve determines the continuous flow of the ink. The valve should open and close according to the design of the print. In the nScrypt 3D direct write dispensing system, the

software converts the design into a code format and then determines the opening and the closing of the valve based on the distance covered by the valve during the printing.

3.1.2 Masking techniques

In the masking technique, a mask is required to make the exact design. The accuracy of the design in the masking technique depends on the mask. The most simple, quick and cost-effective masking technique is brush painting.

3.1.2.1 Brush painting

In the brush painting method, the antenna is manufacturing by dipping the brush in the ink or paste and applying it directly on the substrate [61]. The method is quick however it doesn't offer high accuracy. As it is done by hand, the amount of ink or paste can never be the same whenever the brush is dipped. Usually, a single layer of brush painting is enough to form a thick material surface ranging from 10 µm to 40 µm. Depending on the ink or paste, the brush painting method also requires a post-processing. An illustration of the brush painting method can be seen in Figure. 14.

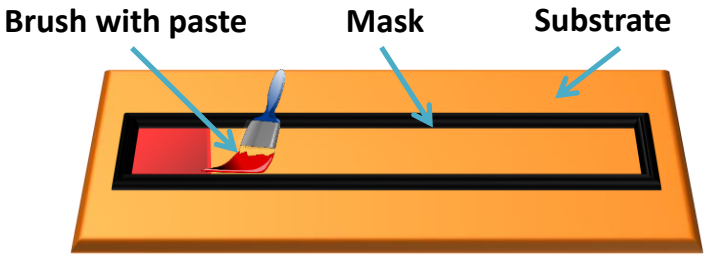

Figure 14: Illustration of brush painting method.

3.1.3 Thermal transfer print (TTP)

Thermal transfer printing is the principle on which thermal printer works [26] [62]. A multi-layer ribbon having thin layer of metal and heat-sensitive acrylic adhesive is installed in the thermal printer. The metal is transferred to the substrate using a thermal print-head which selectively activate the desired regions. Although the method is quick and accurate but there is a chance of wastage of metal. Figure. 15 shows the schematics of thermal printing method.

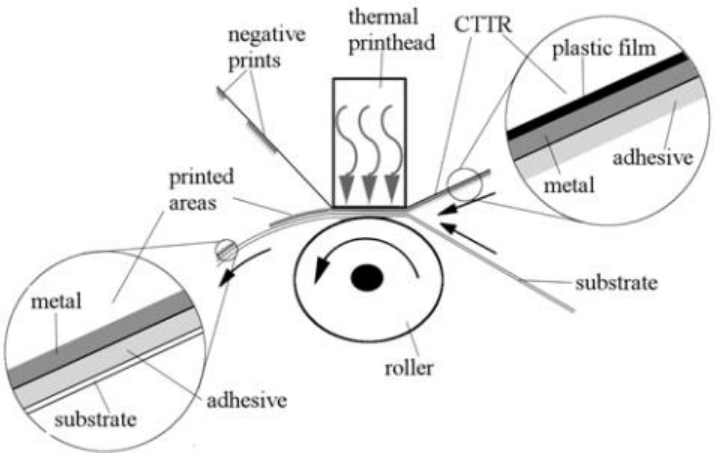

Figure 15: Schematics of thermal printing method.

In this study, Zebra S4M thermal printer is used [63]. The printer has a print-head resolution of 300 DPI and can print at a speed of 5 cm/s. The design can be loaded into the printer using a USB interface. The printing method doesn't require any post-processing and the printed designs are ready to be used immediately. The printer is capable of multi-layer printing but depends highly on the adhesion between the metal and heat-sensitive layer, and the alignment during the multi-layer printing. Figure. 16 and 17 show the Zebra S4M thermal printer and its schematics.

Figure 16: Zebra S4M thermal printer.

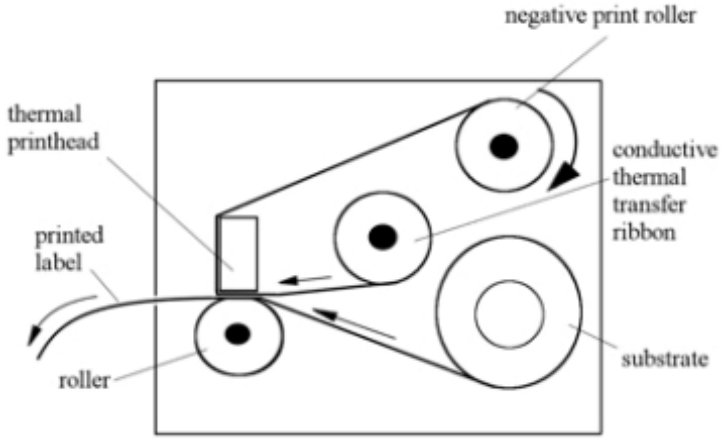

Figure 17: Schematics of Zebra S4M thermal printer.

3.1.4 3D printing

3D printing is the latest manufacturing technology which has gained a lot of interest in research fields including wireless electronics industry. 3D printing can be used to manufacture complex 3D designs by using layer-by-layer deposition of different materials [52] [64]. It is usually used for making substrates as well as conductive designs for antenna applications. The main advantage it offers is customizable structures (shape, size, infill and thickness), electrical properties (dielectric permittivity and loss tangent) and mechanical properties (stretchability, flexibility, weight). Acrylonitrile Butadiene Styrene (ABS) and PolyLactic Acid (PLA) are the most commonly used 3D printable materials [65-67]. Both of these materials are non-flexible however nowadays flexible material such as NinjaFlex is also available for 3D printing. Although there are different types of 3D printers but the most commonly used ones are Fused Deposition Modelling (FDM). Prior to the printing process, the 3D CAD design should be sliced in layers using a 3D printer software or a slicer tool. Figure. 18 shows a simple rectangular patch of 1.2 mm thickness sliced in 6 layers of 0.2 mm each using a slicer tool.

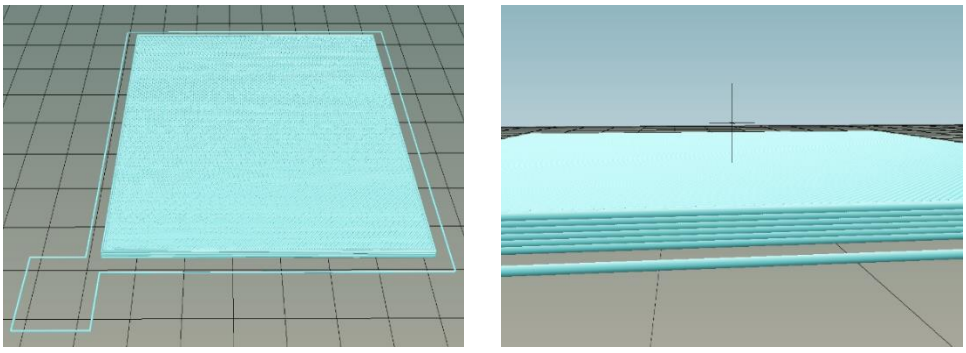

(a) (b)

Figure 18: Spliced rectangular patch (a) Substrate with boundary (b) Side view showing sliced layers.

In FDM based 3D printers [52] [68,69], the material is heated and extruded through the nozzle and onto the base. The 3D printers can have multiple nozzles where one material can be used as the primary and the other can be used as a supporting material. The FDM process is shows in Figure. 19.

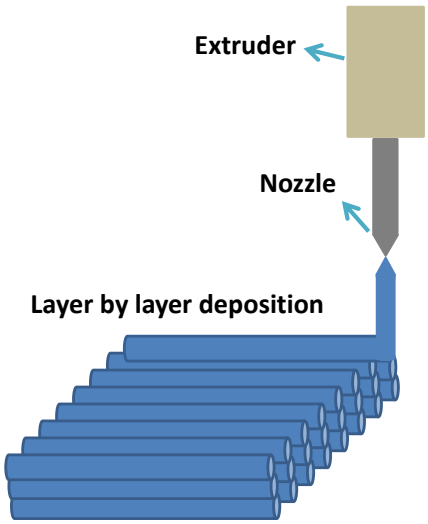

Figure 19: Illustration of FDM process in 3D printers.

In our study, the 3D printing method is used for antenna substrate manufacturing. The printer used is Prenta Duo 3D printer [70] having two 1.75 mm nozzles for printing (Figure. 20). The nozzle can be operated between temperature ranges of 150 - 275 °C. The material commercially comes in the form of a roll called “filament” and it can be installed on the sides of the printer and a plastic tube is used to pass through the material from the roll to the nozzles. The printer has a printing area of 20 x 20 x 20 cm^3. The base plate (bed) is a heatable glass and the temperature can be adjusted for printing different materials. The print quality is effected by several parameters which include the speed of printing, the nozzle and base plate temperature and the nozzle flow.

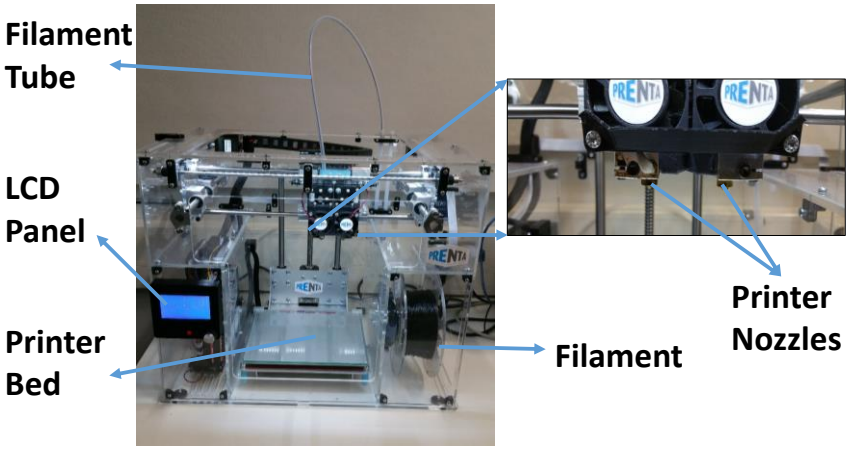

Figure 20: Prenta Duo 3D printer.

3.1.5 Embroidery

Embroidery machines have recently been used for the manufacturing of the antennas [71-73]. It is a good alternative to conductive inks as embroidery utilizes conductive threads. The process is simple, quick and CADs can be easily loaded in the embroidery machines. The substrate fits in the hoop and the embroidery process is done by selecting the design and the stitch types. In this study, the embroidery process is done using Husqvarna Viking embroidery [74] machine shown in Figure. 21.

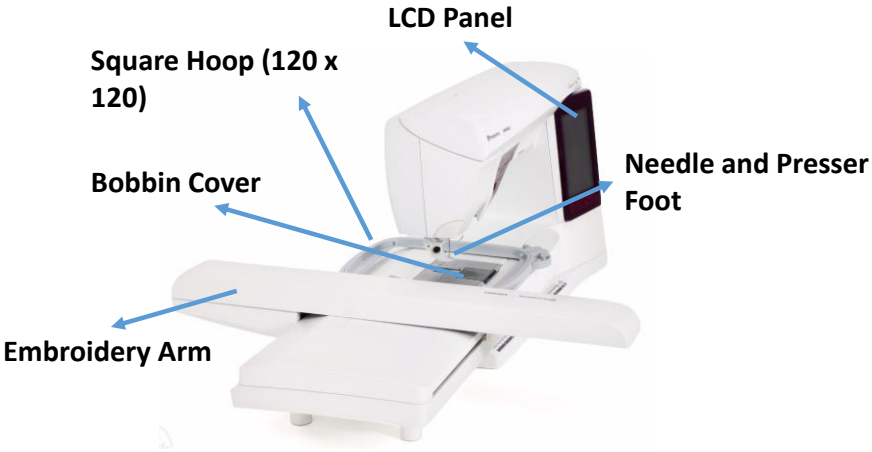

Figure 21: Husqvarna Viking embroidery machine.

3.2 Substrates and conductive materials

3.2.1 Inkjet and thermal printing

The study related to inkjet and thermal printing is done using polyimide substrate (Kapton HN, referred as Kapton or KP) and novel polyester based substrate material (Flexcon THERMLfilm Select 21944E (TC-390), referred as THERMLfilm or TF). Thickness of Kapton and THERMLfilm is 50 µm and 70 µm, and relative permittivities are 3.2 and 3.0 respectively.

For thermal printing, 260 nm thick Al and 340 nm thick Cu film Metallograph™ Conductive Thermal Transfer Ribbons (CTTR) are used as conductor. For inkjet printing, Harima's NPS-JL Ag and ANI Cu-IJ70 Cu nano-particle inks are used. The reason for using Ag and Cu ink is that they are the most widely used nano-particle inks for inkjet printing. The Ag nano-particle ink is expensive but it is easy to post-process using thermal curing at adequate temperatures (100 to 150 °C). On the other hand, Cu nano-particle ink is more conductive and less expensive compared with Ag nano-particle ink but it easily oxidizes in ambient environment resulting in an insulator (Copper oxide).

3.2.2 3D printing

3D printing, in this study, is utilized for making the flexible substrates using NinjaFlex material from Ninjatek. The material has a 200 mm reel diameter and 1.75 mm thread diameter. A single filament costs 50 € and contains approx. 173 meters of material. During the printing process, a single substrate sample utilizes around 1500-2000 mm Ninjaflex material, which means it can print up to 90 substrate samples with one filament making it cost-effective in terms of manufacturing. For the conductive part 3D dispensing and embroidery is used. In 3D dispensing screen printable stretchable Ag conductive paste (DuPont PE872) and in embroidery multifilament Ag plated thread (Shieldex multifilament thread 110f34 dtex 2-ply HC) [75] is used.

3.3 Post-processing

Most of the inks require post-processing before their properties can be modified or improved for using as conductive part of the antenna [52]. The selection of the post-processing method depends on the type of the ink.

3.3.1 Thermal curing

Thermal curing is the most commonly used post-processing method. A conventional oven is used to provide enough temperature for the printed sample so that the organic solvents are removed and conductive particles can stick together and form a conductive surface. The temperature value is set according to the ink and the type of the substrate. If, the ink requires higher temperature but the substrate cannot withstand it then thermal sintering is not used e.g. the Ag nano-particle ink used in our study can be thermally cured however the Cu nano-particle ink required higher reducing temperature and photonic sintering is preferred. The main drawbacks of thermal curing are that it is a slow process and the whole design is exposed to the heating process.

3.3.2 Photonic sintering

Photonic sintering uses high energy pulse light to sinter the conductive material [76]. It is also known as intense pulsed light sintering (IPL). The process is quick and can be applied to selective areas of the printed pattern by adjusting the gap between the mask. Typically photonic sintering systems use Xenon flash lamps for omitting the energy, mask for adjusting the exposure of light to the sample and reflector for focusing the light. A simple photonic sintering system is illustrated in Figure. 22.

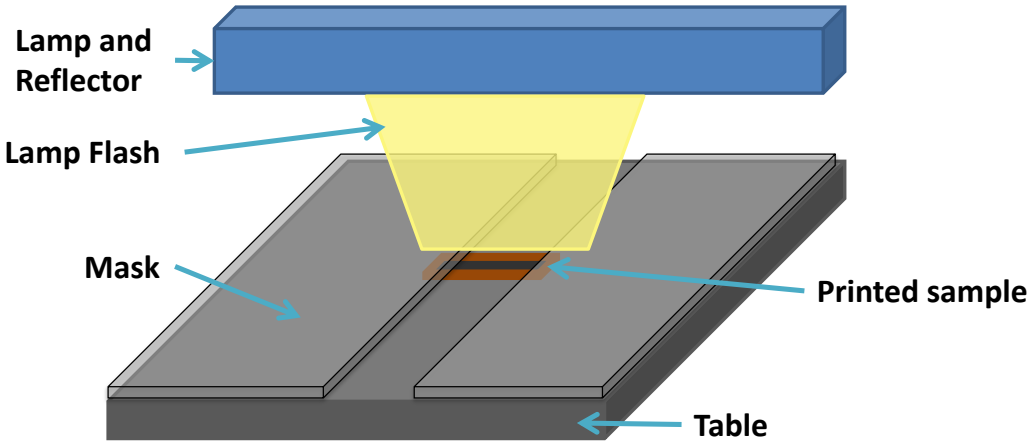

Figure 22: Illustration of a simple photonic sintering system.

The photonic sintering system used in this study is Xenon Sinteron 2010-L system [77]. The specifications of the machine are listed in Table. 2.

Table 2: General properties of Xenon Sinteron 2010-L system

Parameter	Specifications
Lamp	LH-840 Lamp Housing
Pulsed Duration in seconds (s)	100 µs - 2000 µs in increments of 5 µs
Pulse Rate in Hertz (Hz)	1 Hz - 10 Hz in increments of .001 Hz
Pulse Voltage in Volts (V)	1800 V - 3100 V
Pulse Energy in Joules (J)	27 J - 2000 J
Pulse count in numbers	1 - 2000
Aperture ratio	10 mm - 80 mm
Distance between light source and sample	25 mm - 76 mm
Modes	Single, double, continuous and burst

Figure. 23 shows the Sinteron 2010-L rack along with the lamp housing and the sample placing space. The sinteron rack has a power supply, high voltage capacitors and a controller system while the lamp housing, the xenon flash lamp and the cooling system are together on the conveyor table.

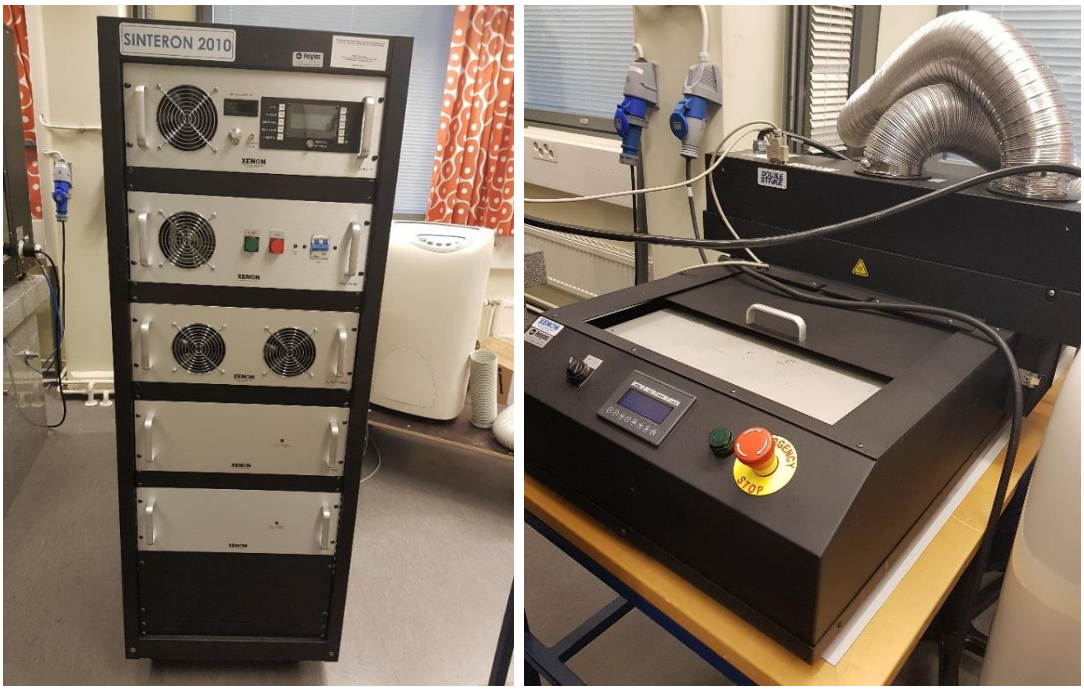

Figure 23: Sinteron 2010-L photonic sintering system.

The energy provided to the sample should be optimized as low energy will not sinter the sample and high energy can damage the sample. Before explaining the energy calculations for the sinteron machine, it is good to understand the different operating modes.

Flash modes

The sinteron machine has four operating modes [77]. The details and the waveforms (Figure. 24-26) are given below:

Single

In single mode, the lamp will flash once when activated. The user can set the pulse voltage and width of the single pulse.

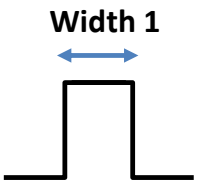

Figure 24: Waveform of single flash mode.

Double

In double mode, the lamp will flash twice when activated. The user can set the pulse voltage, the width of pulse 1 and pulse 2 along with the edge-to-edge gap between both the pulses. The edge-to-edge gap between both the pulses is called the period.

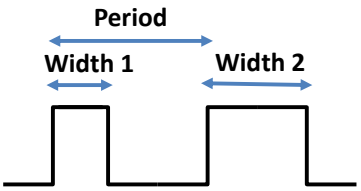

Figure 25: Waveform of double flash mode.

Continuous

In continuous mode, the lamp will keep on flashing until it is stopped using the stop button. The user can set the pulse voltage, the width of the single pulse and the period. This single pulse will then be continuously used during this mode until deactivation.

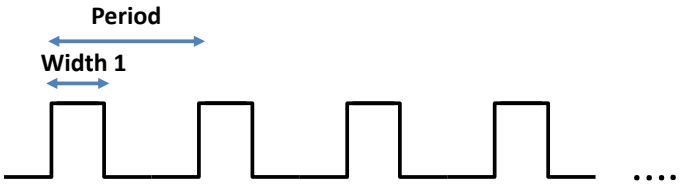

Figure 26: Waveform of continuous flash mode.

Burst

In burst mode, the lamp will flash for a fixed number of times. The user can set the pulse voltage, the width of the single pulse, period and the flash count.

Figure 27: Waveform of burst flash mode.

Energy calculations

The energy present in each pulse can be estimated by using the formula [77]:

$$E = \left(\frac{V}{3120}\right)^{2.4} \times t \ . \tag{13}$$

where, *E* is the energy in joules, *V* the pulse voltage value in volts and *t* the time in microseconds.

3.4 Antenna designs

Three different RFID tag antennas are used for the RFID study [78-80] (Figure. 28-30) and one simple rectangular patch is used for the wearable antenna study (Figure. 31). The purpose of using three different RFID tag antenna designs, which have different structure with narrow and wide tracks, allow an extensive study of printing methods. The design characteristics of three tags are provided in detail in the previous RFID studies [78-80]. All the tag designs can achieve satisfied performance in UHF band (860 MHz to 960 MHz).

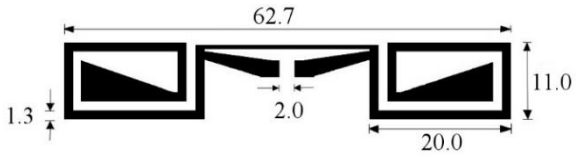

Figure 28: Tag design 1: short dipole-type tag [78].

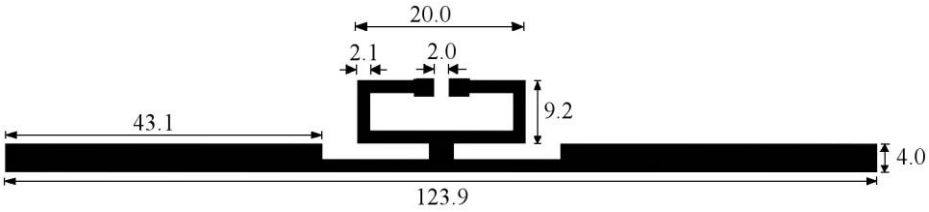

Figure 29: Tag design 2: wideband tag [79].

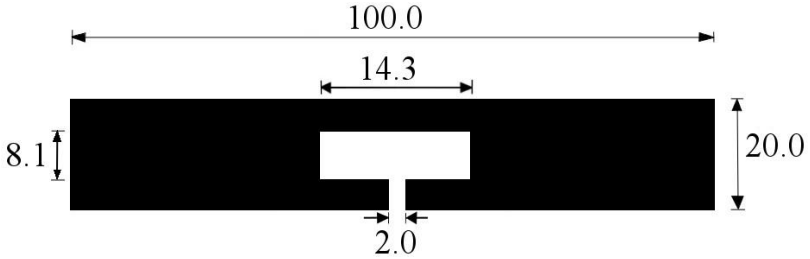

Figure 30: Tag design 3: straight dipole tag [80].

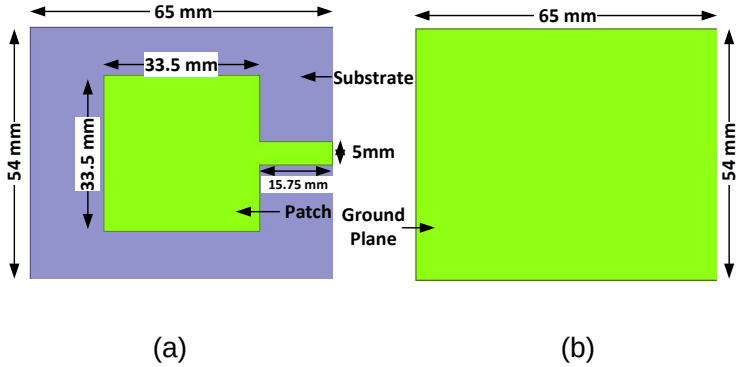

Figure 31: Simple rectangular patch antenna (a) Patch (b) Ground. [Publication V]

3.5 Antenna simulations

The antenna simulations are done using ANSYS HFSS which is a finite element based EM simulator. Two important parameters that are used while simulating the antenna designs are the substrate material properties and the estimated conductivity and thickness of conductor material. The substrate material properties are measured using the Agilent 85070E dielectric probe kit and the conductivity is estimated utilizing the measured DC sheet resistance and the thickness of the conductor. In HFSS model, the substrates are defined as rigid bodies however in reality this is not the case with 3D printed substrate which is one of the differences in simulation and actual measurements. Also, the conductivity and thickness values are estimated and can affect the accuracy of simulations. These can be considered as few uncertainties of the simulations however in all the cases, the simulations are able to present good agreement with the measurement results.

4 Inkjet and thermal printed passive UHF RFID tags

This chapter describes two manufacturing methods, the Inkjet and the thermal printing for the fabrication of passive UHF RFID tags. Section 4.1 and 4.2 highlights the fabrication and reliability testing of Ag based inkjet and Al based thermal printed tags. The work is presented from Publication I and II. Section 4.3 explains the fabrication of Cu based inkjet and thermal printed tags from Publication III and IV.

4.1 Inkjet and thermal transfer printed passive UHF RFID tags

In this study, the comparison of inkjet and thermal printing is done for the manufacturing of passive UHF RFID tags on polyimide (Kapton) and polyester-based substrates (THERMLfilm). The key considerations during the comparison are achieved theoretical read ranges, the ease of fabrication, the flexibility of optimizable parameters and compatibility of different substrates with the printing methods.

For inkjet printing Ag nano-particle ink and for thermal printing Al Metallograph™ CTTR is used. Tag design 1 and 2 are used for this study. Optimization is done for both the printers with each of the substrates. The printed layer thickness is measured using Veeco Wyko NT1100 optical profiling system. The method presented in [81] is used to approximate the sheet resistance and the final achieved conductivities of the inkjet printed samples. For the inkjet printed samples, the final sheet resistance on Kapton and THERMLfilm is calculated to be 56.25 mΩ and 146.12 mΩ. The single layer inkjet printed Ag resulted in 1 µm thick conductor on Kapton and around 0.4 - 0.6 µm on THERMLfilm. The sheet resistance and thickness are used to calculate the achieved conductivity of Ag ink i.e. 1.7×10^7 S/m. For thermal transfer printed samples, the conductivity 2.40×10^7 S/m mentioned by the manufacturer is used. Figure. 32-35 show the printed samples along with microscopic surface pictures.

(a) (b)

Figure 32: Thermal printed Tag design 1 on: (a) Kapton (Al) (b) THERMLfilm (Al).

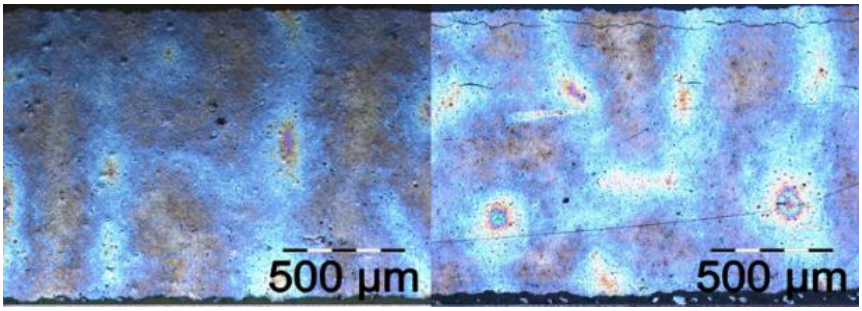

(a) (b)

Figure 33: Microscopic view of Thermal printed Tag design 1 on: (a) Kapton (Al) (b) THERMLfilm (Al). [Publication I]

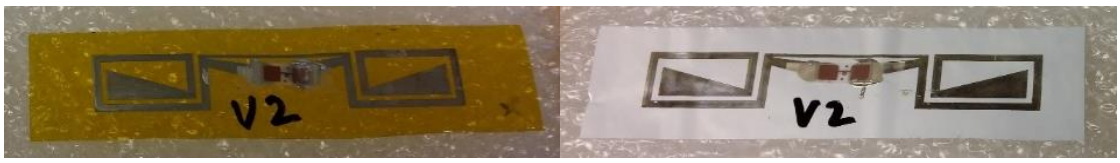

(a) (b)

Figure 34: Inkjet printed Tag design 1 on: (a) Kapton (Ag) (b) THERMLfilm (Ag).

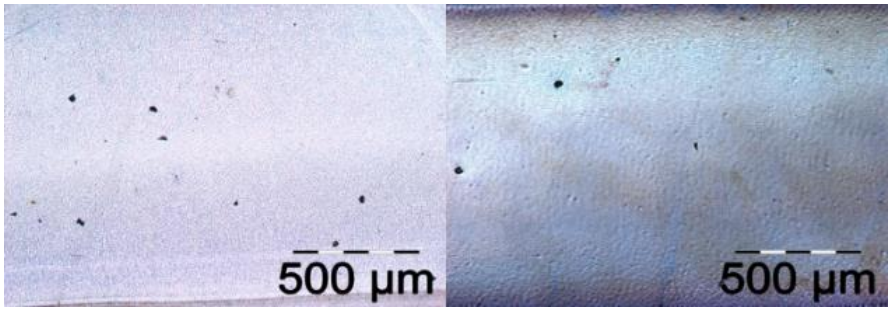

(a) (b)

Figure 35: Microscopic view of Inkjet printed Tag design 1 on: (a) Kapton (Ag) (b) THERMLfilm (Ag). [Publication I]

Figure. 36 and 37 illustrate the simulated and the measured theoretical read range values of the printed RFID tag 1 and tag 2. The peak read ranges of the printed tags are tabulated in Table. 3. The results show that for a particular tag, e.g. Tag 1, similar read ranges for thermal printed tag on different substrates (i.e. Kapton and THERMLfilm) but for the inkjet printed samples the read ranges are quite different. This is because of the ink absorption in inkjet printing, as THERMLfilm is a paper based substrate and absorbs ink. Thus having less conductor thickness and different read ranges. Table. 3 summarizes the measured theoretical read ranges of the fabricated tags.

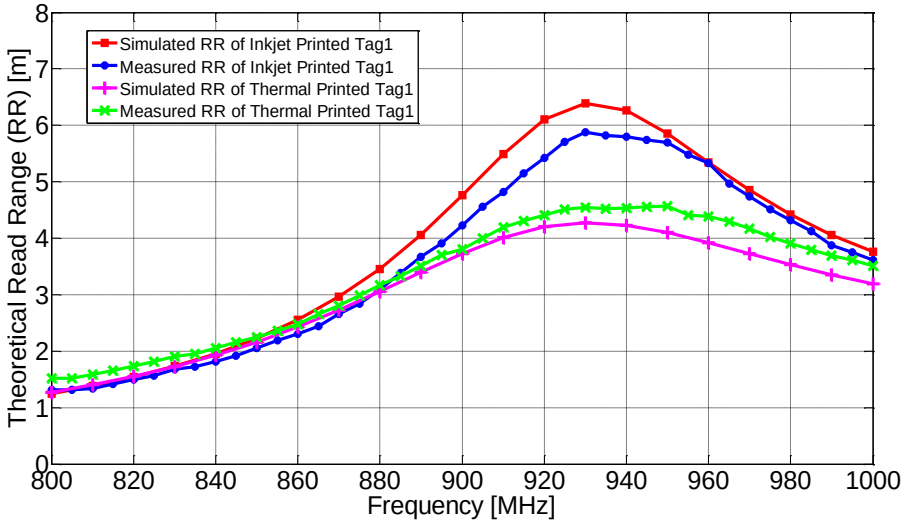

Figure 36: Theoretical read ranges of Tag design 1 on Kapton substrate (Ag for inkjet and Al for thermal printing). [Publication I]

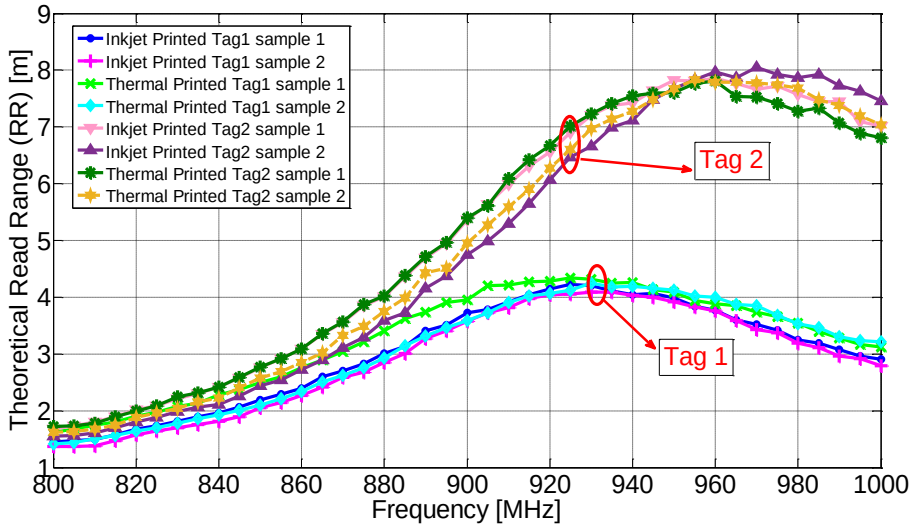

Figure 37: Measured theoretical read ranges of Tag design 1 and 2 on THERMLfilm substrate (Ag for inkjet and Al for thermal printing). [Publication I]

Table 3: Measured theoretical read range. [Publication I]

Printing Method	Substrate	Material	Measured Theoretical Read Range [m]	
			Tag 1	Tag 2
Thermal Printing	Kapton	Al	4.5	Not Available
	THERMLfilm		4.3	7.8
Inkjet Printing	Kapton	Ag	5.8	8.7
	THERMLfilm		4.2	8.0

In thermal transfer print, the most important aspect is the successful transfer of the conductor to the substrate. This limits the type of substrates the thermal transfer print supports. This is very clear from the experiment as we are not able to have a successful printing of Tag 2 on Kapton using thermal transfer print. Even for Tag 1 multiple tries are done before a tag design was successfully printed although the design still had some missing conductive parts. This is due to the poor adhesiveness of thermal ribbon on Kapton as shown in Figure. 38.

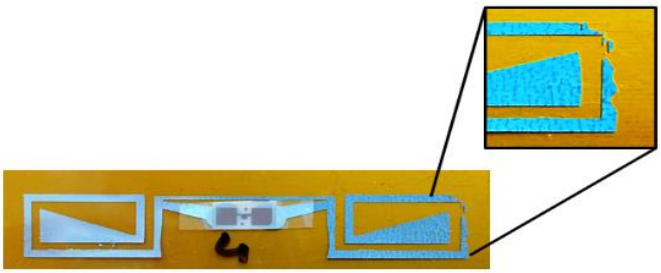

Figure 38: Adhesion problem with thermal printing on Kapton. [Publication I]

4.2 Reliability of inkjet and thermal transfer printed passive UHF RFID tags in high humidity conditions

In this work, the reliability of Inkjet and thermal transfer printed passive UHF RFID tags is studied on THERMLfilm substrates with Tag design 2. A regular textile glue (Gutermann Creativ HT2, referred as Glue 1) and a normal superglue (Loctite Super Glue, referred as Glue 2) are used to protect the IC during the humidity test. Two glues are used to mitigate the effects of glue type on the tag performance. The tag performance is measured in different conditions i.e. after fabrication, after applying coating, immediately after the test and then after drying for 24 hours.

As seen from the Figure. 39, both the glues have no effect on the read range of the inkjet printed tag however, glue 1 shifts the peak read range frequency to lower values. The tag antenna impedance and ohmic losses are affected during the test and thus a shift in frequency is observed immediately after the test. After 24 hours, the performance returns to normal. These results are appropriate for many wireless applications where humidity/moisture can be a concern.

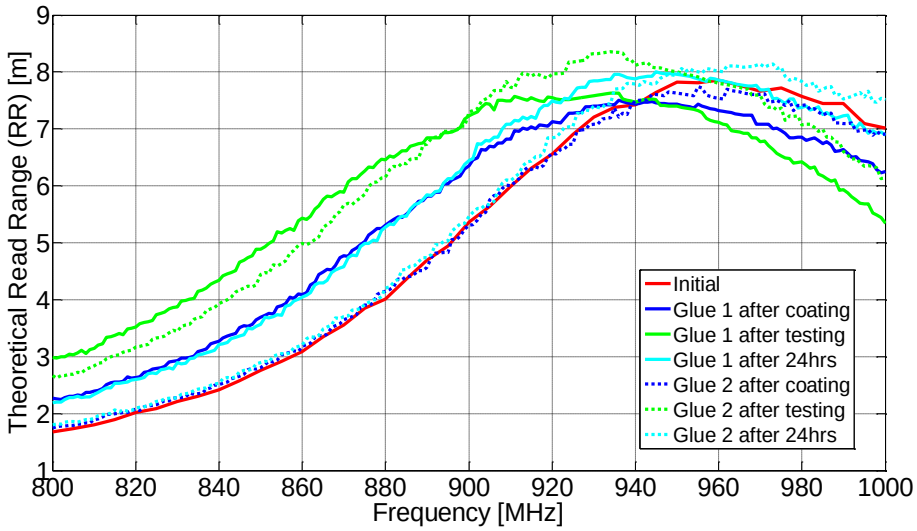

Figure 39: Effects of high humidity on measured theoretical read ranges of Inkjet printed tags. [Publication II]

On the other hand, the thermal printed tags (Figure. 40) are effected by glue 1 and the peak read range decreases from 7.8 m to about 5.5 m. After the test, the peak read range decreases to 4 m and after 24 hours it further decreases to about 2-3 m. In case of glue 2, the read range slightly decreases from 7.8 m to 7 m after applying the glue. Moisture and drying have similar effect in case of glue 2 in thermal printed tags as in the inkjet printed tags.

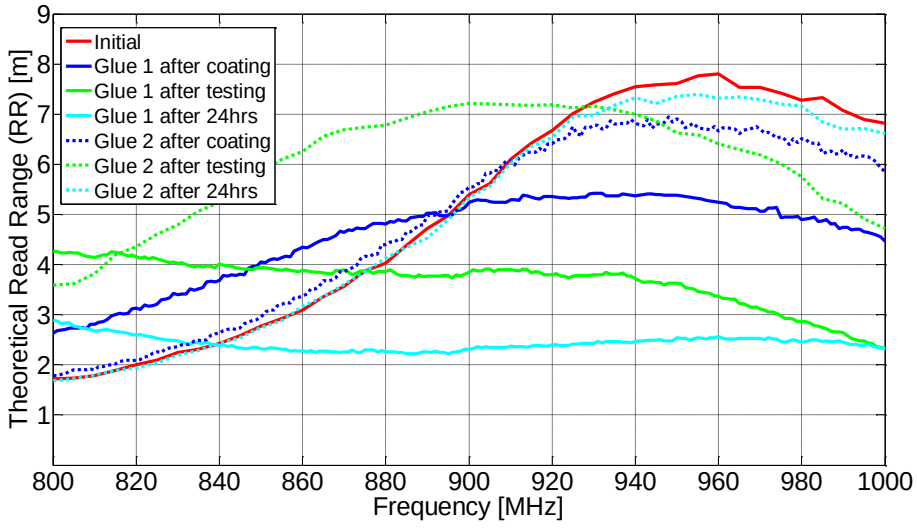

Figure 40: Effects of high humidity on measured theoretical read ranges of Thermal printed tags. [Publication II]

After the test, the surface of the inkjet printed tags is not affected but the thermal printed tags clearly show rough surface and the conductor dissolved from some spots. Figure. 41 show the surface of thermal printed samples from two different spots before and after the test. The results indicated that

the inkjet printed tags can withstand the high humidity conditions regardless of the glue used however in case of thermal printed tags the most important challenge is to find a suitable coating for the tags to maintain their performance in high humidity conditions.

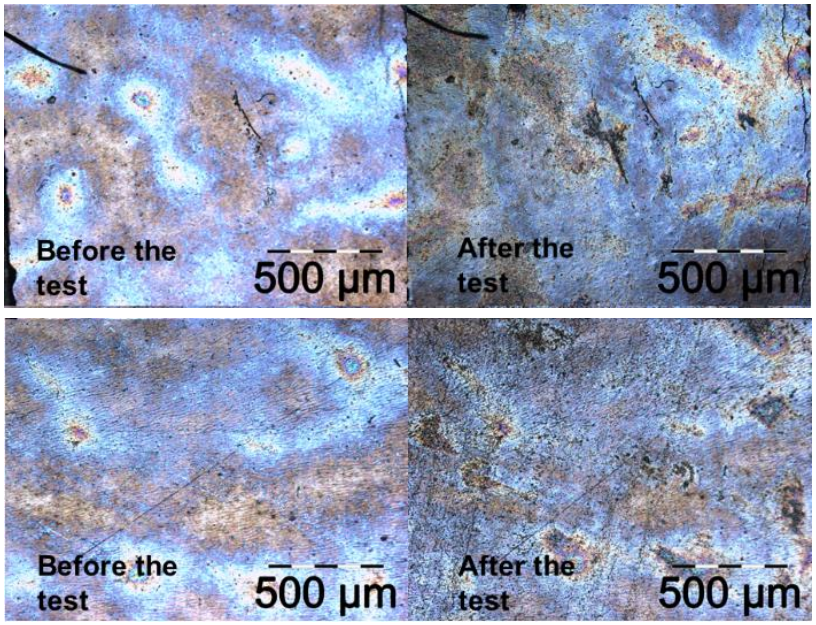

Figure 41: Surface of a Thermal printed antenna before and after test from two different parts. [Publication II]

4.3 Cu based inkjet and thermal transfer printed passive UHF RFID tags

The performance of Cu based inkjet and thermal printed RFID tags are compared in Publication III and IV with three different tag designs. Using Cu as conductive material reduces the cost of production as Ag based inks are expensive. Previously, inkjet and screen printed Cu conductor is cured using laser curing on different substrates [82]. The printing process remains the same as in previous studies however in case of inkjet printing, the printed tags are post processed using photonic sintering.

For thermal printed Cu tags, a 340 nm thick Cu film is used. Figure. 42 and 43 show the printed samples along with microscopic surface pictures and surface roughness. The Cu traces have an RMS roughness of 19.8 nm whereas the Al traces have RMS roughness of 20.8 nm. Both the traces have smoother surfaces when compared with inkjet Ag traces on THERMLfilm. The thermal printed Cu antennas achieved conductivity of 3.9×10^7 S/m. The conductivity measurement is explained in detail in Publication III.

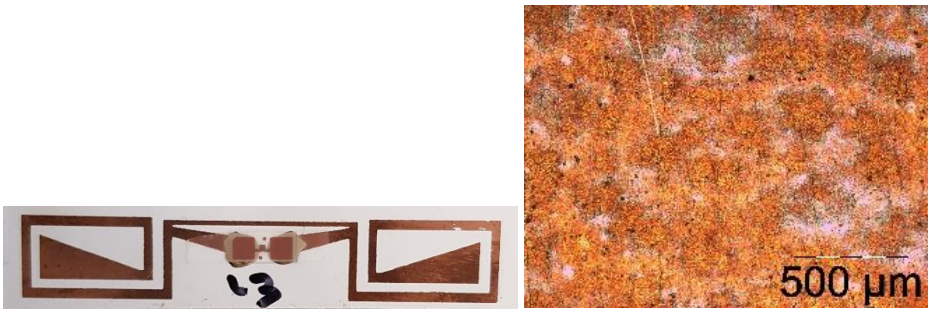

(a) (b)

Figure 42: Ready tag: (a) Thermal printed Cu tag (b) Microscopic picture of the surface. [Publication III].

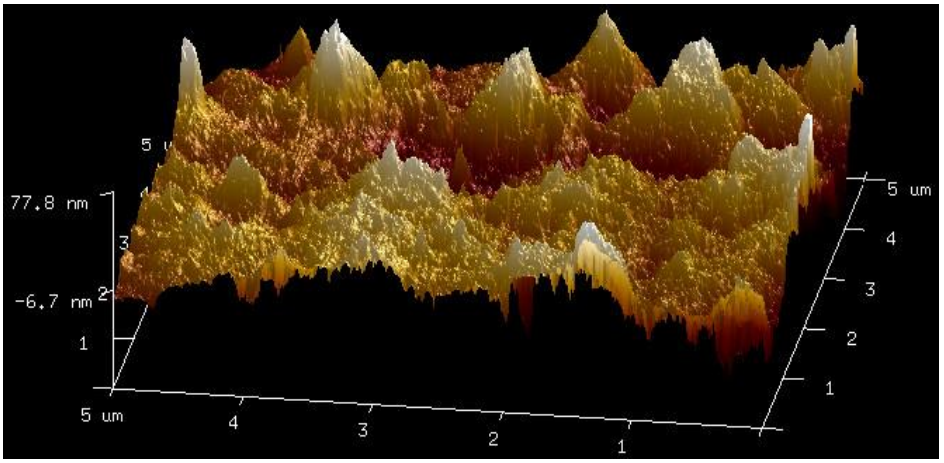

Figure 43: Thermal printed Cu trace surface morphology. [Publication III]

The tag performance is evaluated through wireless tag measurements under the European RFID transmission regulations as explained in Section 2.5. Figure. 44-46 show the read range of three different thermal printed Cu tags compared with the tags fabricated in the previous studies (Al and Ag based). For tag design 1, Thermal printed Cu antennas achieved maximum read range of 6.6 m which is 2.2 m better than thermal printed Al antennas. This is due to the higher conductivity of Cu traces and thick metallic layer. The thermal printed Cu antennas also managed to have a read range improvement of 0.8 m over the inkjet printed antennas on Kapton and 1.7 m over the inkjet printed antennas on THERMLfilm.

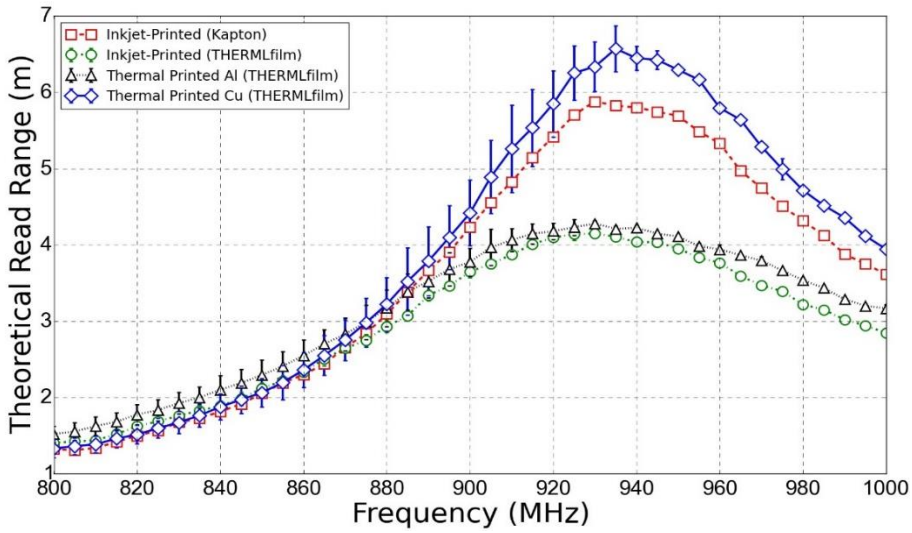

Figure 44: Measured theoretical read ranges of Tag design 1 (Ag for Inkjet printed samples). [Publication III]

Tag design 2 and 3 show similar improvement in the read range of Cu antennas due to their higher conductivity and thick metallic layer. For tag design 2, Thermal printed Cu antennas achieved maximum read range of 9.0 m which is 1.3 m better than thermal printed Al antennas. Similarly, the thermal printed Cu antennas managed to have a read range improvement of 0.4 m over the inkjet printed antennas on Kapton and 1.1 m over the inkjet printed antennas on THERMLfilm.

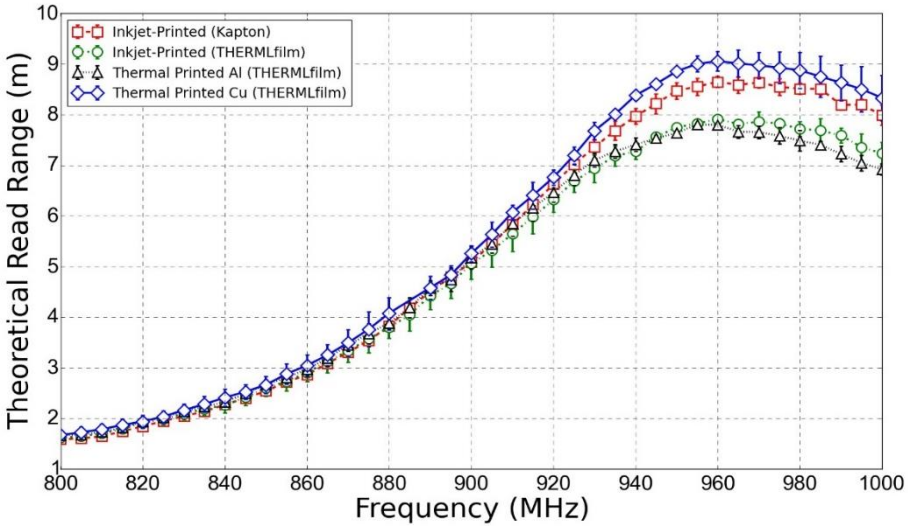

Figure 45: Measured theoretical read ranges of Tag design 2 (Ag for Inkjet printed samples). [Publication III]

For tag design 3, Thermal printed Cu antennas achieved maximum read range of 10.6 m which is 0.8 m better than thermal printed Al antennas. The Cu antennas showed 1.4 m read range improvement over the inkjet printed antennas on THERMLfilm but in case of the inkjet printed antennas on Kapton, the read range is very similar with Cu antennas having a little shift in the frequency.

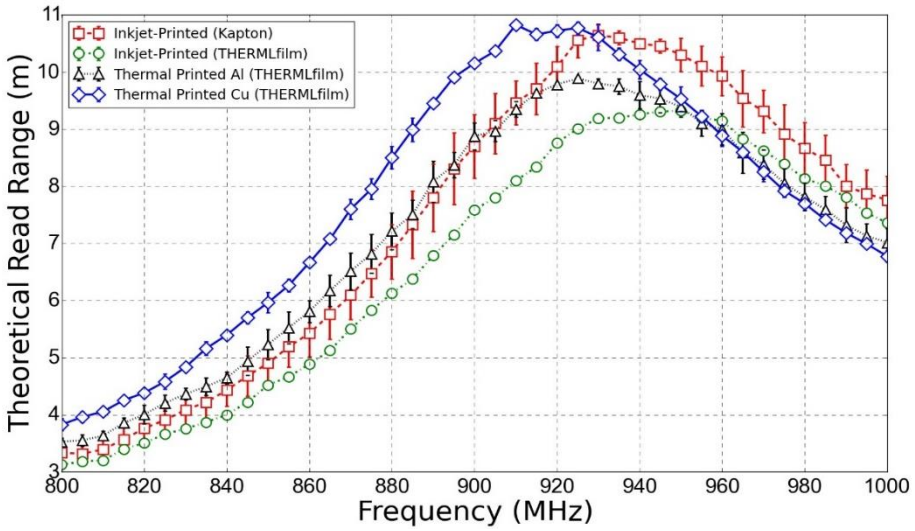

Figure 46: Measured theoretical read ranges of Tag design 3 (Ag for Inkjet printed samples). [Publication III]

Publication IV focuses on fabricating Cu based RFID tags with photonic sintered inkjet printing and comparing them to the tags fabricated in Publication III. The printing parameters for Cu were optimized during the printing process. Higher platen temperature tends to have a greater effect on the print quality due to quick absorbing and drying of the ink which resulted in cracks on the printed layer. This phenomena can be seen in Figure. 47. In the previous studies, when printing Ag, higher temperature was used and there was no such effect on the printed layer. The details of optimized printing parameters can be found in Publication IV table I. The printed samples are heat sintered for 30 minutes at 100 °C before photonic sintering as recommended by the manufacturer.

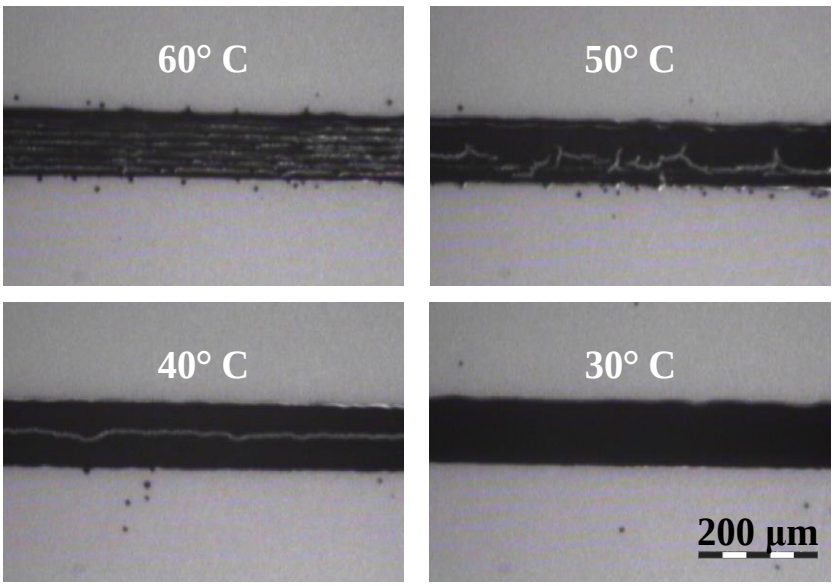

Figure 47: Effect of platen temperature on Inkjet printed Cu pattern. [Publication IV]

Section 3.2.2 explains in detail about the photonic sintering and the machine i.e. Xenon Sinteron 2010-L used for it. Voltage and pulse duration should be optimized for every substrate and conductive material. One flash of 2200 V with 1700 us pulse duration sintered the Cu on Kapton substrates however on THERMLfilm substrate, even after using different combinations of flashes and pulse duration resulted in non-conductive surface or partial removable of Cu layer as seen in Figure. 48. The reason for non-conductive is insufficient amount of energy transferred to properly sinter the Cu. Increasing the energy resulted in the removal of the printed ink from the surface of THERMLfilm substrate due to low adhesion of the ink on it. Multiple layers of Cu (2-6 layers) were also printed as a test but similar results are produced during the sintering process. To improve the adhesion, oxygen plasma treatment using Diener Pico equipped with optional RIE (Reactive-Ion Etching) style electrodes was performed. The parameters were optimized for THERMLfilm substrate as mentioned in Publication IV. However, no improvement was observed during the sintering process and the sintering process failed to produce conductive layers. This concluded that the photonic sintering is not suitable for THERMLfilm with the inkjet printed Cu nano-particle ink. The conductivity of the inkjet-printed Cu on Kapton was found to be around 1.50×10^{7} S/m.

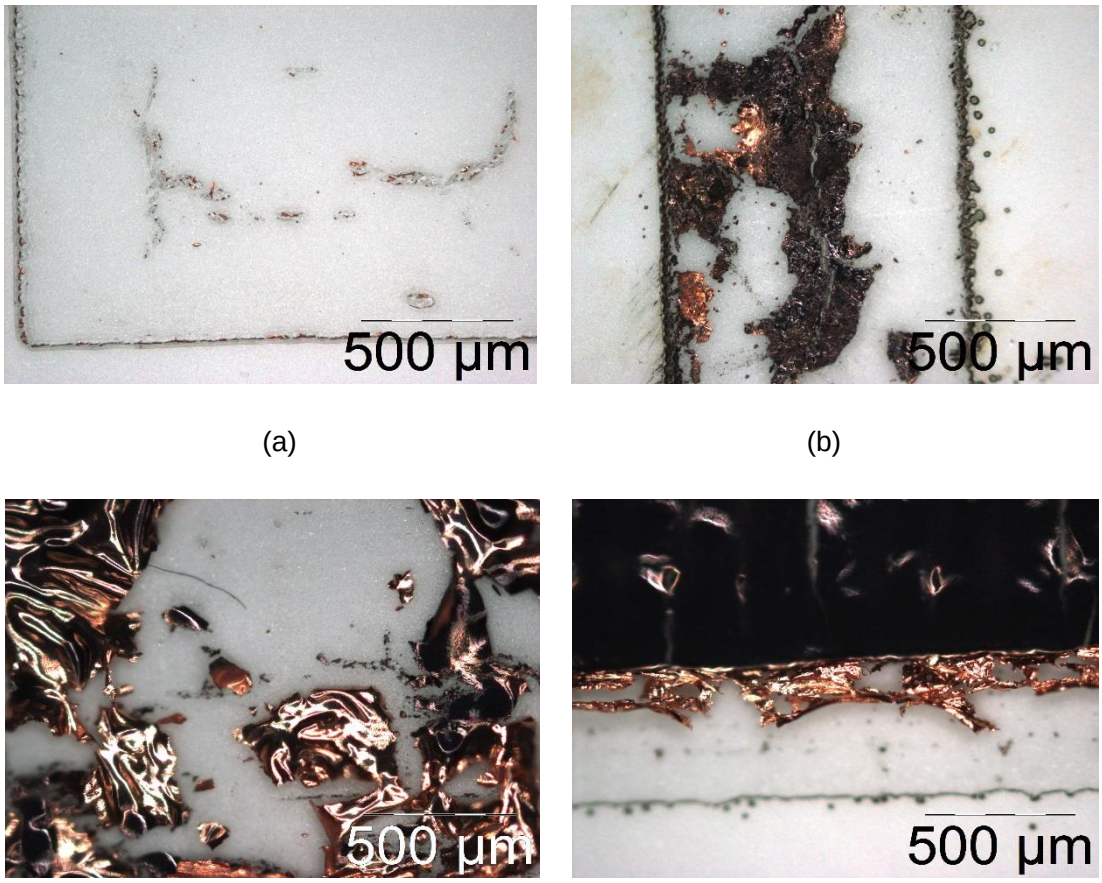

Figure 48: Printed pattern after sintering with (a) 2200 V, 1700 µs (b) 2000 V, 1500µs (c) 2000 V, 1300 µs (d) 1800 V, 1000 µs. [Publication IV]

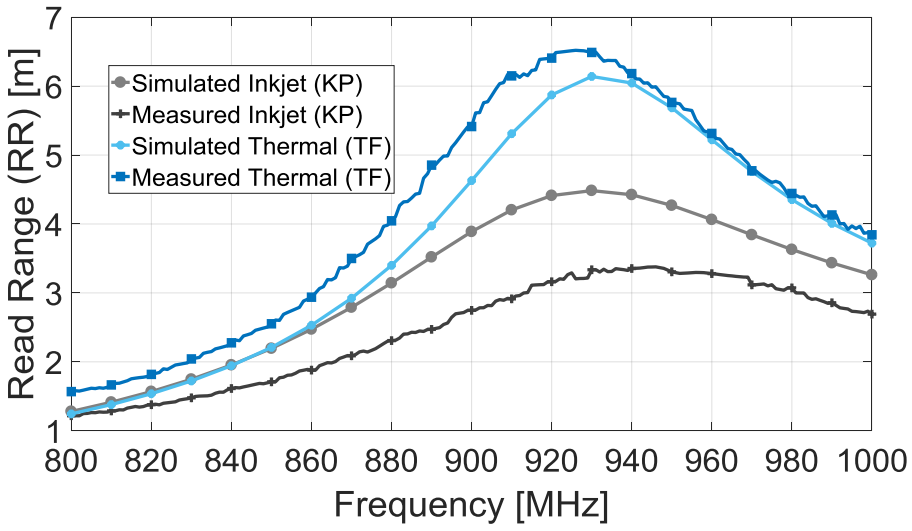

Figure 49: Theoretical read ranges of Tag design 1 with Cu material.

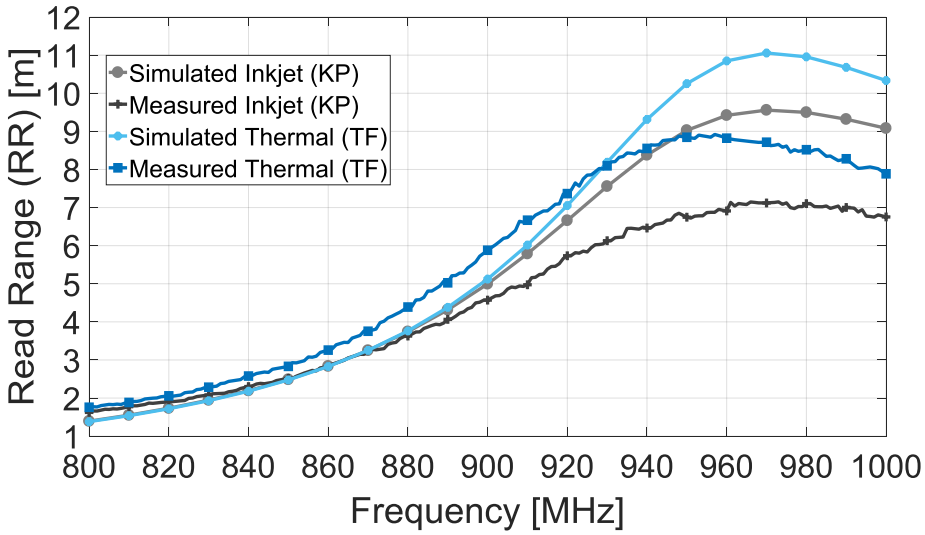

Figure 50: Theoretical read ranges of Tag design 2 with Cu material.

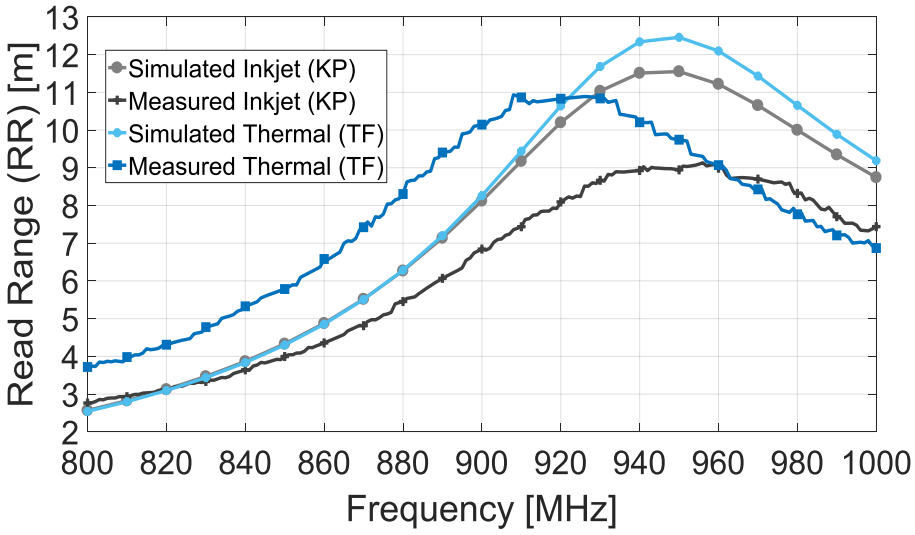

Figure 51: Theoretical read ranges of Tag design 3 with Cu material.

Figure. 49-51 show the simulated and measured read ranges of Cu based inkjet printed tags on Kapton and thermal printed tags on THERMLfilm.

Table. 4 summarizes the measured theoretical read ranges of all the printed tags in Publication I, III and IV.

Table 4: Comparison of printed tags in this study and previous studies. [Publication IV]

Publication	Method, substrate	Material	Tag 1	Tag 2	Tag 3
[I, III]	Thermal Transfer Print (Kapton)	Al	Fabrication not successful		
[III, IV]		Cu			
[I, III]	Thermal Transfer Print (THERMLfilm)	Al	4.4 m	7.7 m	9.8 m
[III, IV]		Cu	6.6 m	9.0 m	10.6 m
[III, IV]	Inkjet Print (Kapton)	Ag	5.8 m	8.6 m	10.6 m
[IV]		Cu	3.4 m	7.1 m	10.8 m
[III, IV]	Inkjet Print (THERMLfilm)	Ag	4.2 m	7.9 m	9.2 m
[IV]		Cu	Fabrication not successful		

5 3D printing for development of wearable antenna and passive UHF RFID tag

This chapter highlights the development of wearable antenna and passive UHF RFID tags on 3D printed NinjaFlex substrate. Brush painting, 3D dispensing and embroidery process is used for fabricating the conductive part on 3D printed NinjaFlex substrate in Publication V, VI and VII, respectively.

5.1 Brush painting wearable antenna on a 3D printed substrate

In this study, the proof of concept of fabricating the flexible antenna by brush painting stretchable Ag conductive paste on 3D printed substrate is presented. A simple rectangular patch antenna with dimensions optimize to resonate around 2.45 GHz and 2.5 GHz in industrial, scientific, and medical (ISM) band is used. Brush painting is used as a simple and quick method to fabricate the antenna on 1.2 mm thick 3D printed NinjaFlex substrate. 3D printing for substrate and brush painting for antenna fabrication is explained in detail in Publication V. The brush painting is done using a simple brush and stencil made according to the antenna design. After brush painting, the stretchable Ag conductive paste is thermally cured at 110 °C for 15 minutes. The fabricated antenna is shown in Figure. 52.

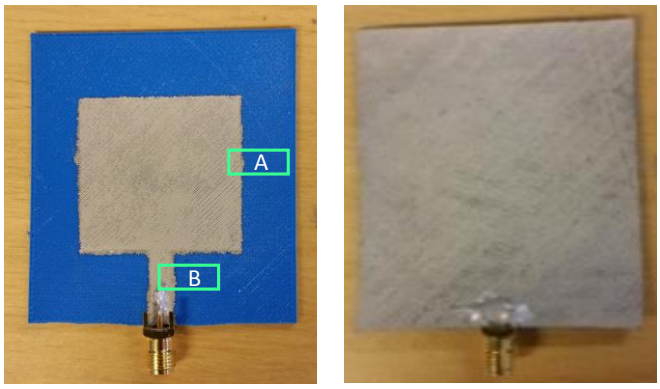

(a) (b)

Figure 52: Fabricated antenna (a) Patch (b) Ground. [Publication V]

Microscopic pictures of substrate before and after the brush painting (Figure. 53) shows a continuous conductor that covers the substrate surface very well. Brush painting inaccuracy can be seen in Figure. 6 of Publication V. The conductor forms a thick layer with an average of 26.52 µm calculated using the cross sectional view of the fabricated antenna as seen in Figure. 54. The measured conductivity is approx. 1.7×10^4 S/m. The properties of the fabricated samples are listed in table I of Publication V.

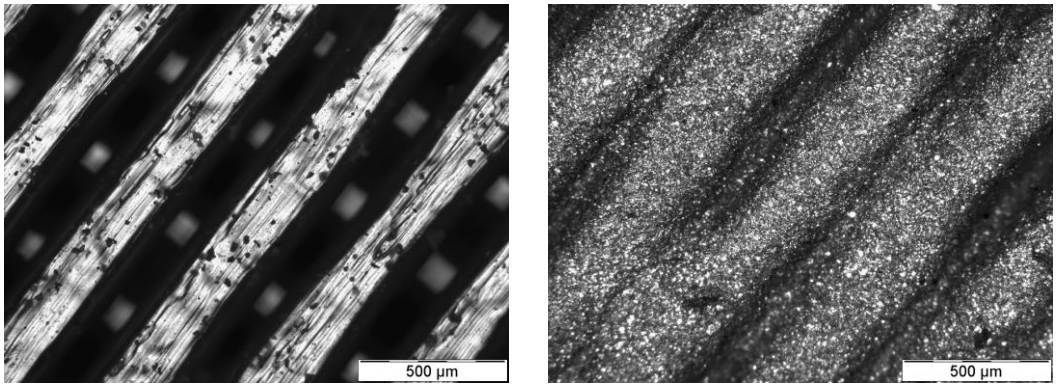

(a) (b)

Figure 53: Surface of the substrate material (a) top view before brush painting (b) top view after brush painting and thermal curing. [Publication V]

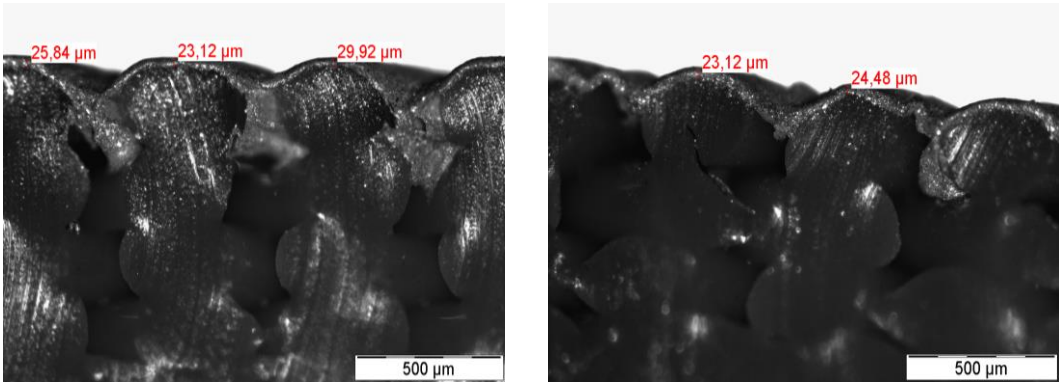

(a) (b)

Figure 54: Conductor thickness from cross-sectional view of the fabricated antenna. [Publication V]

The simulations for the fabricated antenna are completed using ANSYS HFSS ver. 15 in free space and near a human body model presented in [83]. Results in Figure. 2 of Publication V show a slight decrease in the reflection coefficient near the body model when compared with free space. Overall the performance is similar in both simulations because the full ground plane of the antenna minimizes the effects of the human body. After fabrication, the bending test is performed which represents the normal environment of a wearable antenna because human body parts are not flat and the wearable antenna is typically placed on the arms and the legs etc. Bending test and its procedure is explained in detail in Publication V. Figure. 55 shows the reflection coefficient in flat and different bend conditions (simulations and measurements). The results show that there is a shift in frequency slightly to a lower values. The antenna does operate at 2.45 GHz in all the studied cases. Table. 5 summarizes the simulation and measurement results of the bending test.

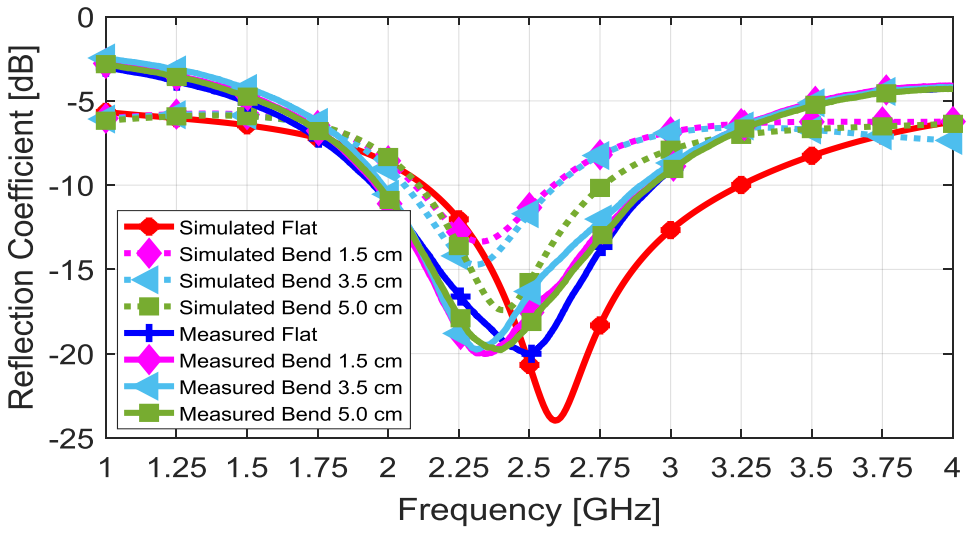

Figure 55: Reflection coefficient [dB] of antenna in flat and bent conditions. [Publication V]

Table 5: Effects of antenna bending. [Publication V]

Antenna Position	Reflection Coefficient at 2.45 GHz [dB]	Bandwidth [MHz]	Minimum Reflection Coefficient at [GHz]
Simulated (S) [Flat]	-18.28	1120 MHz (2.13 GHz – 3.25 GHz)	2.59
S Bending 1.5 cm	-12.15	480 MHz (2.10 GHz – 2.58 GHz)	2.32
S Bending 3.5 cm	-12.72	540 MHz (2.06 GHz – 2.60 GHz)	2.31
S Bending 5.5 cm	-16.98	650 MHz (2.11 GHz – 2.76 GHz)	2.41
Measured (M)[Flat]	-19.68	990 MHz (1.94 GHz – 2.93 GHz)	2.50
M Bending 1.5 cm	-18.57	960 MHz (1.96 GHz – 2.92 GHz)	2.33
M Bending 3.5 cm	-17.61	910 MHz (1.98 GHz – 2.89 GHz)	2.32
M Bending 5.0 cm	-19.15	970 MHz (1.96 GHz – 2.93 GHz)	2.40

Figure. 56 shows the simulated and measured radiation pattern in 2D yz-plane for studied cases of flat and different bend conditions. Results show an increase in the beam width and decrease in directivity with the increase in bending. Figure. 12 of Publication V presents the effect of bending on the total efficiency of the fabricated antenna. The overall frequency is similar for the smaller bendings but for the larger bending (1.5 cm) a slight increase is observed. The peak gain of the antenna does not change and larger bending decreases the directivity thus increasing the total efficiency. For the smallest bending (5 cm) the slight decrease in efficiency is due to the decreased matching as compared to the flat antenna. After the bending test, no cracks are observed on the surface of the antenna under microscope and the performance returned to normal in the end.

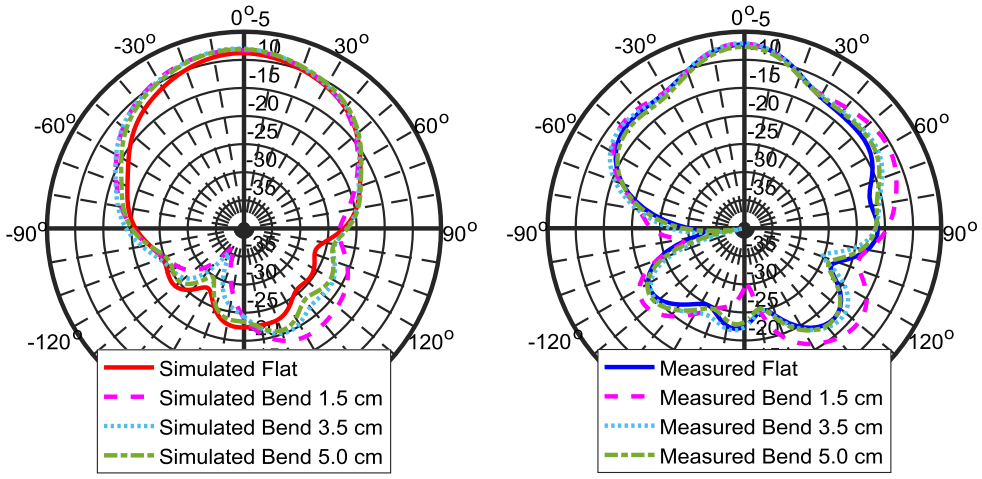

(a) (b)

Figure 56: 2D radiation pattern of the antenna (a) Simulated (b) Measured. [Publication V]

Specific Absorption Rate (SAR) simulations are done near skin block of 18.75x18.75x30 cm^3 located at a distance of 5 mm from the antenna with 1 W power supplied to the antenna, as in the reference [84]. The antenna clearly follows U.S. Federal Communications Commission (FCC) regulation as the SAR value is 0.368 W/kg which is well within the SAR_{max} limit of 1.6 W/kg. Overall, the results show that this fabrication methods and materials can be used for the integration of antennas on versatile flexible 3D printed structures. The method is simple, quick and customization of 3D adds versatility for antenna manufacturing for future wearable applications.

5.2 Flexible and stretchable 3D printed passive UHF RFID tag

The work presents a stretchable 3D printed passive UHF RFID tag. The substrate, NinjaFlex, is 3D printed using a Prenta 3D printer and then stretchable Ag conductive paste is dispensed on it. The characterisation of printed substrate at UHF band is done with Agilent 85070E dielectric probe kit. The characterisation method and results are explained in detail in Publication VI. The substrate has an average dielectric relative permittivity of 2.84 and a loss tangent of 0.065. Figure. 57 shows the measurement setup and the measured results of the sample.

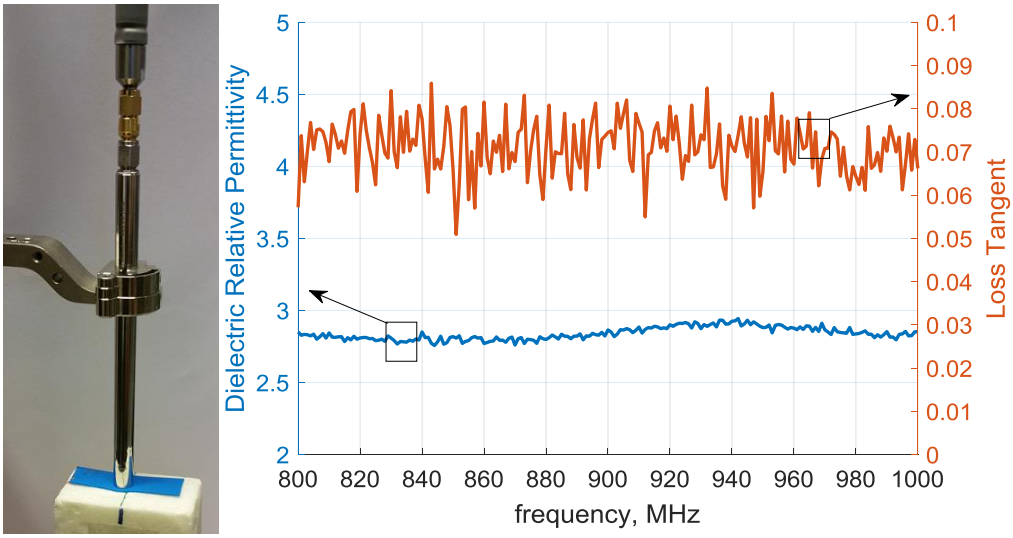

Figure 57: Material characterisation setup and results. [Publication VI]

Nscrypt 3D dispenser is used for printing the stretchable paste. The dispenser has variety of tip sizes which are used depending on the viscosity of the material. The paste has higher viscosity and thus the largest tip with 125 µm size along with 18 psi pump pressure is used during the dispensing. These settings let the paste flow continuously and the antenna design is printed accurately. A single layer of paste is dispensed and then sintered for 15 minutes at 110 °C. In the end NXP UCODE G2iL RFID IC is attached to the tag antenna terminals. Figure. 58 shows the fabricated tag along with the microscopic picture of the tag surface.

(a) (b)

Figure 58: Ready Tag (a) Top view (b) Microscopic view of surface. [Publication VI]

Table 6: Measured properties of fabricated tag. [Publication VI]

Thickness (µm)	Sheet resistance (mΩ/sq)	Resistivity (Ω.m)	Conductivity (S/m)
39.5	15.5	6.122×10^{-7}	1.633×10^{6}

Table. 6 shows the measured properties of the fabricated tag. These properties are used to estimate the simulation shown in Figure. 59. A Stretching test is designed in which the tag is stretched 5 mm from both ends 100 times and the wireless performance is measured after every few stretches. Figure. 59 shows the results from the stretching test along with the simulations. Initially, the tag showed the peak read range of 10.6 m at 920 MHz while at the end of the test, the peak read range dropped to 7.4 m which is enough to make it suitable for the RFID identification and sensing applications. The stretching test did not effect the frequency of peak read range and it stayed at 920 MHz for all measurements. Overall, there is a 30 % decrease in the peak read range and the realized gain drops around 2.82 dB. The peak read range and the realized gain value at each measurement is given in table 2 of Publication VI.

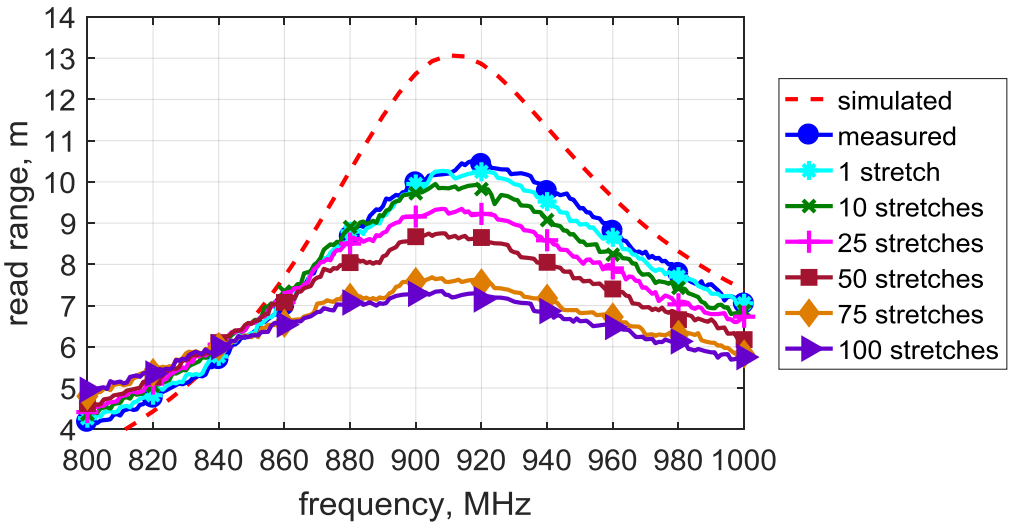

Figure 59: Theoretical read range of the Tag: Simulated, measured before and after the test. [Publication VI]

Figure. 60 shows the tag after the stretching test along with the microscopic picture of its surface. No cracks or permanent elongation is observed after the test and the tags can be considered for the applications requiring endurance to strain. The overall efficiency of the antenna is estimated to be around 48% which is better than the antenna efficiency in Publication V. This improved efficiency is due to the dispensing fabrication method.

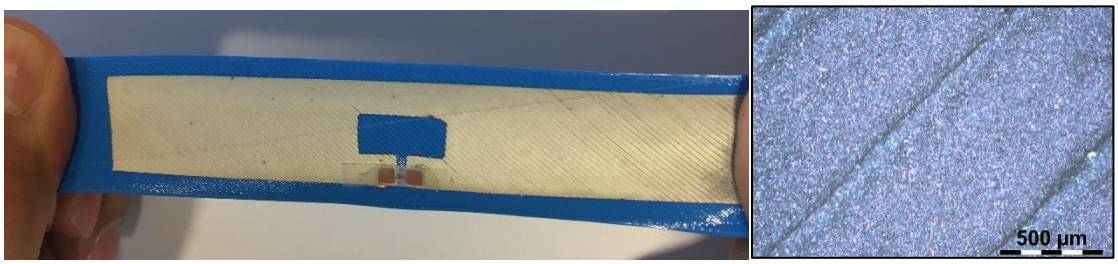

(a) (b)

Figure 60: Tag after the stretching test (a) While stretched (b) Microscopic image of surface. [Publication VI]

5.3 Embroidered passive UHF RFID tag on flexible 3D printed substrate

Hybrid fabrication methodology for the manufacturing of a passive UHF RFID tag is presented in Publication VII. The hybrid fabrication proposed in this study is the combination of 3D printing and embroidery process. Similar to Publication V and VI, 3D printing is used to make the substrate in this publication, however, the conductor is not printed instead a Multifilament Ag plated thread is embroidered to make the tag design. The details of 3D printing the NinjaFlex substrate is given in Publication VII along with the material characterisation at UHF band. The material characterisation is done in the similar way as explained in Publication VI. The only difference is that the substrate thickness i.e. 0.5 mm in this study. The thickness is kept low so that the needle of embroidery machine can easily penetrate the substrate without breaking. The substrate has average dielectric relative permittivity of 1.87 and loss tangent of 0.036.

The ready tag can be seen in Figure. 61 along with microscopic pictures from the top showing the Ag thread and from the back showing the knots. The NXP UCODE G2iL RFID IC is then attached to the tag antenna terminals and the wireless measurements are taken after the joint is dried. Figure. 62 (a) shows the measured read range of three fabricated samples of same design along with the simulations. The substrate characterisation (dielectric and loss tangent) and Ag plated thread (DC lineal resistivity and thickness) values are used in the simulations to estimate it with more accuracy.

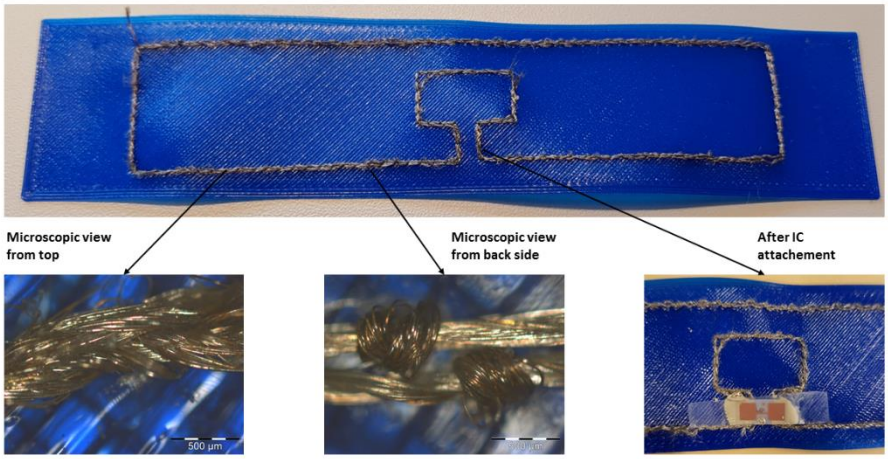

Figure 61: Ready Tag along with microscopic surface images. [Publication VII]

In simulation the tag achieves a peak read range of 5.90 m at 930 MHz, while the three fabricated samples show peak read ranges of 5.92 m, 5.83 m and 5.85 m at 925 MHz, 918 MHz and 914 MHz, respectively. Figure. 62 (b) shows the simulated and the measured realized gain patterns of the fabricated samples at 930 MHz. Table. 7 summarizes the peak read range and the realized gain values as seen in the simulation and measurements. Overall the results are in good matching. Based on the results, it is evident that the combination of 3D printing and embroidery can be used for cost and time effective manufacturing of the passive UHF RFID tags for flexible wireless platforms.

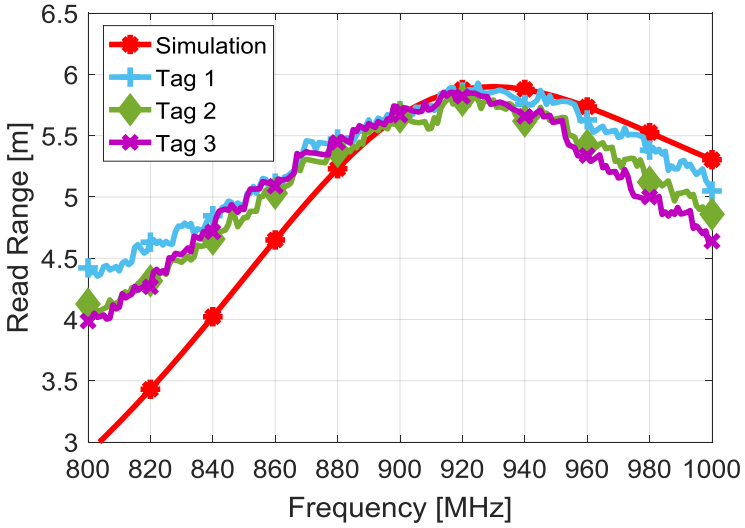

(a)

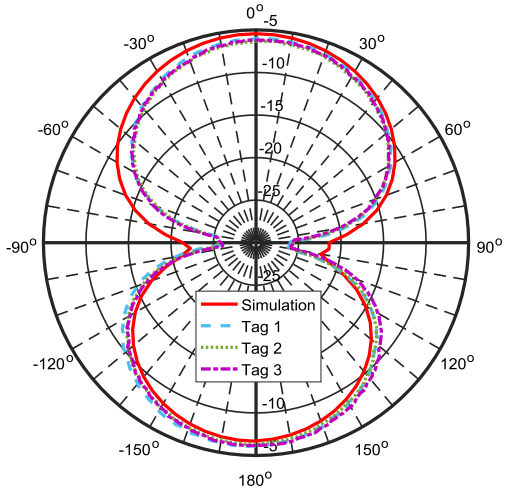

(b)

Figure 62: Simulated and measured results (a) Theoretical read range in meters, (b) Realized gain in dB at 930 MHz. [Publication VII]

Table 7: Summary of simulated and measured results of the samples. [Publication VII]

Tag Under Study	Peak Read Range [m]	Frequency of Peak Read Range [MHz]	Realized Gain at 930 MHz [dBi]
Simulation	5.90	930	-5.44
Tag 1	5.92	925	-5.90
Tag 2	5.83	918	-6.19
Tag 3	5.85	914	-6.15

5.4 Comparison of manufacturing methods

Table. 8 summarizes all the manufacturing methods used in the thesis with respect to cost, manufacturing time and results in general.

Table 8: General comparison of manufacturing methods.

Manufacturing Method	Equipment Cost	Conductor Cost	Post-Processing	Time to Produce Single Sample	Achieved Conductivity
Inkjet Printing	High	Ag Ink = 1000 $/100g Cu Ink = 700 $/100g	Required	10 minutes to print and 1 hour for post-processing	Ag Ink = $1.7x10^7$ S/m Cu Ink = 1.50×10^7 S/m
Thermal Printing	Low	< 500 $/Ribbon	Not Required	Single sample can be printed in seconds	Al Ink = $2.40x10^7$ S/m Cu Ink = 3.9×10^7 S/m
Brush Painting	Low	1000 $/250g	Required	Manual process and can take upto 5-10 minutes to print and then 15 minutes to post-process	Ag Paste = 1.7×10^4 S/m
3D Dispensing	Very High	1000 $/250g	Required	10 minutes to print and 15 minutes for post-processing	Ag Paste = $1.6x10^6$ S/m
Embroidery	Low	200 $	Not Required	5-10 minutes	Ag Thread = 1×10^4 S/m

6 Conclusions

The thesis focused on finding out how the selected novel materials and manufacturing methods are combined to produce low-cost, robust, efficient and reliable passive UHF RFID tags for future wireless applications. The research work is done on material as well as the antenna part for improving the overall manufacturing of RFID tags. The results show that novel approaches can be made to fabricate quick, cost-effective and reliable wireless components for sensing and wearable applications.

The first objective of the thesis was achieved and presented in the Publication I-IV. The comparison of inkjet and thermal printing was done for the manufacturing of passive UHF RFID tags on two different substrates. The results showed that inkjet printing can print on different substrates like polyimide and polyester-based substrates however in thermal printing the range of compatible substrate is limited by the adhesion of CTTR on the substrate. The inkjet printed tags outperformed the thermal printed tags in case of theoretical read ranges. Afterwards, reliability test was done on tags printed on THERMLfilm. Two different glues were used to coat the tag IC. The results indicated that the inkjet printed tags can withstand the high humidity conditions regardless of the glue used however in case of thermal printed tags, the performance decreased.

The work was extended using Cu based inkjet and thermal printed passive UHF RFID tags. The reason for using Cu based ink is that it is cheaper than the silver ink and can give comparable results and a cost-effective solution for manufacturing RFID tags. The main challenge in using the Cu is that it requires high temperature for reduction. The substrates under test cannot withstand such high temperatures thus photonic sintering was used as a post-processing method for inkjet printed tags. According to the results, the Cu based tags showed better performance as compared to the previously printed

tags. However photonic sintering was not able to produce a conductive trace on THERM-Lfilm with the inkjet printed Cu nano-particle ink even after improving the adhesion with oxygen plasma treatment.

The second objective, development of flexible 3D printed passive UHF RFID tags and wearable antennas, was achieved in the work presented in Publication V-VII. Initially, proof-of-concept of fabricating flexible antenna on the 3D printed NinjaFlex substrate by brush painting stretchable Ag conductive paste was studied. NinjaFlex material is flexible, customizable and inexpensive. The paste adds more flexibility to the antenna for adopting the wearable environment near human body. The performance of the antenna was tested in flat and bend conditions and the results showed that the antenna can operates well in all of them. The antenna also satisfied the SAR limit imposed by U.S FCC regulations.

The final conductivity and the efficiency of the antenna was low but better wireless properties were observed by using 3D dispensing with the same material and fabricating a flexible and stretchable 3D printed passive UHF RFID tag. The novelty of the work included the characterisation of 100% infill rectilinear printed Ninjaflex for complete UHF band, dispensing stretchable silver paste and then studying the impact of stretching on the tag's performance. The fabricated tag was stretched multiple times and wireless measurements were done. Results showed that the tags can withstand extreme stretching and peak read range (10.56 m) dropped around 30 % (7.35 m) after 100 stretches. No cracks or permanent elongation was observed after the test and the tags showed great potential to be used in applications that require endurance to strain. In the end, hybrid fabrication methodology was proposed by the combination of 3D printing and embroidery process for the manufacturing of passive UHF RFID tags. Only the contour or the outer boundary of the design was embroidered and the tag showed 5.92 m peak read range which is very good as compared to the tag performance in previous studies considering that less conductor was used by the embroidery process. The results showed that the methodology can be used for cost and time effective RFID fabrication along with suitable performance for wireless sensing applications.

6.1 Major contributions of the thesis

As mentioned earlier, the thesis contributes towards the novel manufacturing methods for the development of passive UHF RFID tags and wearable antennas on versatile substrates. Few of the major contributions of the thesis are:

1. Exploring thermal printing for the fabrication of passive UHF RFID tags on Kapton and THERMLfilm substrates with different conductive materials.
2. Comparison of inkjet printing and thermal printing for the fabrication of passive UHF RFID tags and their reliability study in high humidity conditions.
3. 3D printing and characterizing flexible NinjaFlex substrate with different thickness, i.e. 1.2 mm and 0.5 mm, at UHF band. Utilizing NinjaFlex as substrate for RFID and wearable antenna study.
4. Brush painting stretchable conductive paste for the manufacturing of wearable antenna on 3D printed substrate.
5. Manufacturing flexible and stretchable 3D printed passive UHF RFID tag. The results of the tag show that it can be used as a sensor in applications where strain is a concern.
6. Embroidered passive UHF RFID tag on 3D printed substrate. The tag maintained good performance with only a contour design of the tag and can be used as wearable sensor in body area networks.

6.2 Future research recommendations

All the research done in this thesis is mostly based on experiments. The results are very promising however there are certain aspects that still need further research such as:

1) Exploring more suitable substrates for thermal printing.
2) 3D printing of substrate with different infills and its effect on the antenna performance.
3) Exploring flexible conductive materials that can be 3D printed on NinjaFlex.

Huge potential lies in these fabrication methodologies and with optimization for specific substrate or customized printed substrate, overall fabrication process can be improved in terms of time, cost and efficiency. Results obtained in this dissertation provide a path-way for benefiting from the manufacturing methods to produce better smart products for future wireless applications.

References

[1] X. Jia, Q. Feng, T. Fan, and Q. Lei, “RFID technology and its applications in Internet of Things (IoT),” *Proc. Int. Conf. Consum. Electron. Commun. Netw. (CECNet)*, pp. 1282-1285, Apr. 2012.

[2] KuBo, “The research of IoT based on RFID technology,” *International Conference on Intelligent Computation Technology and Automation*., pp. 832-835, Jan. 2015.

[3] S. Dominikus, M.J. Aiger, and S. Kraxberger, “Passive RFID technology for the Internet of Things,” *International Conference for Internet Technology and Secured Transactions (ICITST)*, pp. 1-8, Nov. 2010.

[4] K. Finkenzeller, “*RFID H*andbook: Radio-Frequency Identification Fundamentals and Applications” Wiley, New York, 2003.

[5] D. Dobkin, “*The RF in RFID: passive UHF RFID in practice*” Elesvier, New York, 2007.

[6] R. Want, “An introduction to RFID technology,” *IEEE Pervasive Computing*, vol. 5, no. 1, pp. 25-33, Mar. 2006.

[7] F. J. Valente and A. C. Neto, “Intelligent steel inventory tracking with IoT / RFID,” *IEEE International Conference on RFID Technology & Application (RFID-TA)*, pp. 158-163, Nov. 2017.

[8] D. Zhang, L. T. Yang, M. Chen, S. Zhao, M. Guo, and Y. Zhang, “Realtime locating systems using active RFID for Internet of Things,” *IEEE Syst. J.*, vol. 10, no. 3, pp. 1226-1235, Sep. 2016.

[9] G. Xiao, P. Aflaki, S. Lang, Z. Zhang, Y. Tao, C. Py, P. Lu, C. Martin and S. Chang, “Printed UHF RFID Reader Antennas for Potential Retail Applications,” *IEEE Journal of Radio Frequency Identification*, Apr. 2018.

[10] P. Bilski et al., “Application of the RFID technology in the European Union border control system,” *IEEE International Conference on RFID Technology & Application (RFID-TA)*, pp. 28-33, Nov. 2017.

[11] S. Karuppuswami, L. L. Matta, E. C. Alocilja and P. Chahal, “A wireless RFID compatible sensor tag using gold nanoparticle markers for pathogen detection in the liquid food supply chain,” *IEEE Sensors Letters*, Apr. 2018.

[12] S. Javaid, A. Sufian, S. Pervaiz and M. Tanveer, “Smart traffic management system using Internet of Things,” *International Conference on Advanced Communication Technology (ICACT)*, pp. 393-398, Mar. 2018.

[13] A. Vena, L. Sydänheimo, L. Ukkonen and M. M. Tentzeris, “A fully inkjet-printed chipless RFID gas and temperature sensor on paper,” *IEEE RFID Technology and Applications Conference (RFID-TA)*, pp. 115-120, Oct. 2014.

[14] R. Baccarelli, G. Orecchini, F. Alimenti and L. Roselli, “Feasibility study of a fully organic, CNT based, harmonic RFID gas sensor,” *IEEE International Conference on RFID-Technologies and Applications (RFID-TA)*, pp. 419-422, Jan. 2012.

[15] I. Jauregi et al., “UHF RFID Temperature Sensor Assisted With Body-Heat Dissipation Energy Harvesting,” *IEEE Sensors Journal*, vol. 17, no. 5, pp. 1471-1478, Mar. 2017.

[16] M. C. Caccami, M. P. Hogan, M. Alfredsson, G. Marrocco and J. C. Batchelor, “A Tightly Integrated Multilayer Battery Antenna for RFID Epidermal Applications,” *IEEE Transactions on Antennas and Propagation*, vol. 66, no. 2, pp. 609-617, Feb. 2018.

[17] S. Yang, M. Crisp, R. V. Penty and I. H. White, “RFID Enabled Health Monitoring System for Aircraft Landing Gear,” *IEEE Journal of Radio Frequency Identification*, Apr. 2018.

[18] X. Hui and E. C. Kan, “Mitigation of body movement interference in near-field coherent sensing for heartrate monitoring,” *IEEE International Conference on Wearable and Implantable Body Sensor Networks (BSN)*, pp. 156-159, Apr. 2018.

[19] F. Calignano et al., “Overview on additive manufacturing technologies,” *Proc. IEEE*, vol. 105, no. 4, pp. 593-612, Apr. 2017.

[20] S. A. Nauroze et al., “Additively manufactured RF components and modules: Toward empowering the birth of cost-efficient dense and ubiquitous IoT implementations,” *Proceedings of the IEEE*, vol. 105, no. 4, pp. 702-722, Apr. 2017.

[21] L. Yang, A. Rida, R. Vyas and M. M. Tentzeris, “RFID tag and RF structures on paper substrates using inkjet-printing technology,” *IEEE Transactions on Microwave Theory and Techniques*, vol. 55, no. 12, pp. 2894-2901, Dec. 2007.

[22] M. M. Tentzeris, K Sangkil, A. Traille, H. Aubert, K. Yoshihiro, A. Georgiadis and A. Collado, “Inkjet-printed RFID-enabled sensors on paper for IoT and “Smart Skin” applications,” *International Conference on Applied Electromagnetics and Communications (ICECom)*, pp. 1-4, Oct. 2013.

[23] S. Kim, Y. Kawahara, A. Georgiadis, A. Collado, and M. M. Tentzeris, “Low-cost inkjet-printed fully passive RFID tags for calibrationfree capacitive/haptic sensor applications,” *IEEE Sensors J.*, vol. 15, pp. 3135-3145, Jun. 2015.

[24] R. Singh, E. Singh and H. S. Nawla, “Inkjet printed nanomaterial based flexible radio frequency identification (RFID) tag sensors for the internet of nano things,” *RSC Advances*, Issue 77, pp. 48597-48630, Sept. 2017.

[25] Y. Ren, J. Virkki, L. Sydänheimo and L. Ukkonen, “Optimisation of manufacturing parameters for inkjet-printed and photonically sintered metallic nanoparticle UHF RFID tags,” *Electronics Letters*, vol. 50, no. 21, pp. 1504-1505, Octo. 2014.

[26] M. Kgwadi, C. J. Vourch, D. J. Harrison and T.D. Drysdale, “On-demand printing of antennas for TV white-space communications,” *Loughborough Antennas and Propagation Conference (LAPC)*, pp. 553-556, Nov. 2014.

[27] K. V. Hoel, S. Kristoffersen, J. Moen, K. G. Kjelgård and T. S. Lande, “Broadband antenna design using different 3D printing technologies and metallization processes,” *European Conference on Antennas and Propagation (EuCAP)*, pp. 1-5, Jun. 2016.

[28] S. H. Naushahi, K. Rasilainen and V. Viikari, “Realization of RFID tag antenna with 3D printing technology,” *European Conference on Antennas and Propagation (EuCAP)*, pp. 1-4, Jun. 2016.

[29] B. Sanz-Izquierdo and J. Sungyun, “WLAN antenna on 3D printed bracelet and wrist phantom,” *Loughborough Antennas and Propagation Conference (LAPC)*, pp. 372-375, Dec. 2014.

[30] W. G. Whittow, “3D printing, inkjet printing and embroidery techniques for wearable antennas,” *European Conference on Antennas and Propagation (EuCAP)*, pp. 1-4, Jun. 2016.

[31] M. Ahmadloo and P. Mousavi, “Application of novel integrated dielectric and conductive ink 3D printing technique for fabrication of conical spiral antennas,” *IEEE Antennas and Propagation Society International Symposium*, pp. 780-781, Jul. 2013.

[32] M. Attaran, “The rise of 3-D printing: The advantages of additive manufacturing over traditional manufacturing,” *Business Horizons*, vol. 60, Issue 5, pp. 677-688, 2017.

[33] Harima NPS-JL silver nanoparticle ink, https://www.harima.co.jp/en/products/electronics/pdf/brochure16e_23.pdf (Accessed on 12th Jan 2018)

[34] ANI Cu-IJ70 Cu nanoparticle ink, http://nebula.wsimg.com/f356531a3cd44d6939147efb4932fed6?Access-KeyId=D6756B5639AB3254C10B&disposition=0&alloworigin=1 (Accessed on 12th Jan 2018)

[35] DuPont PE872 http://www.dupont.com/ (Accessed on 12th Jan 2018)

[36] K. Finkenzeller, “*RFID Handbook: Fudamentals and Applications in Contactless Smart Cards and Identification*” West Sussex: John Wiley & Sons Ltd., 2003.

[37] R. Das and P. Harrop, “*RFID forecasts, players and opportunities 2011-2021*” IDTechEx, 2011.

[38] V. D. Hunt, A. Puglia and M. Puglia, "*RFID-A Guide to Radio Frequency Identification*" Hoboken, NJ: Wiley, 2007.

[39] A.B. Constantine, "*Antenna Theory: Analysis and Design*", 3rd ed., John Wiley & Sons, Inc. 2005.

[40] J.D. Kraus, "*Antennas for All Applications*", 3rd Edition, USA, McGraw-Hill. 2002. 921 p.

[41] W. Stutzman and G. Thiele, "*Antenna Theory and Design*", 2nd ed., Hoboken, New Jersey: John Wiley & Sons, Inc., 1998.

[42] K. Kurokawa, "Power waves and the scattering matrix," *IEEE Transactions on Microwave Theory and Techniques*, vol. 13, no. 2, pp. 194-202, Mar. 1965.

[43] P. Nikitin, K. Rao, S. Lam, V. Pillai, R. Martinez and H. Heinrich, "Power reflection coefficient analysis for complex impedances in RFID tag design," *IEEE Transactions on Microwave Theory and Techniques*, vol. 53, no. 9, pp. 2721-2725, Sept. 2005.

[44] P. Nikitin, K. Rao, R. Martinez and S. Lam, "Sensitivity and impedance measurements of UHF RFID chips," *IEEE Transactions on Microwave Theory and Techniques*, vol. 57, no. 5, pp. 1297-1302, Mar. 2009.

[45] G. Marrocco, "The art of UHF RFID antenna design: impedance-matching and size-reduction techniques," *IEEE Antennas and Propagation Magazine*, vol. 50, no. 1, pp. 66-79, Apr. 2008.

[46] K. Rao, P. Nikitin and S. Lam, "Antenna design for UHF RFID tags: a review and a practical application," *IEEE Transactions on Antennas and Propagation*, vol. 53, no. 12, pp. 3870-3876, 2005.

[47] V. Cerbek, C. Steger, R. Weiss, J. Preishuber-Pflügl and M. Pistauer, "A UHF measurement and evaluation test system," *Elektrotechnik & Informationstechnik*, Vol. 124, No. 11, pp. 384-390, Oct. 2007.

[48] K. V. S. Rao, P. V. Nikitin and S. F. Lam, "Impedance matching concepts in RFID transponder design," *IEEE Workshop on Automatic Identification Advanced Technologies*, ser. AUTOID '05, pp. 39-42, Dec. 2005.

[49] NXP UCODE G2iL IC Datasheet, http://www.nxp.com/documents/data_sheet/SL3S1203_1213.pdf (Accessed on 12th Jan 2018).

[50] T. Björninen, L. Sydänheimo and L. Ukkonen, "Development and validation of an equivalent circuit model for UHF RFID IC based on wireless tag measurements," *Antenna Measurement Techniques Association Symposium*, 21-26 Oct., 2012, Bellevue, WA.

[51] J. Virtanen, J. Virkki, L. Sydänheimo, M. Tentzeris, and L. Ukkonen, "Automated identification of plywood using embedded inkjet-printed passive UHF RFID tags," *IEEE Transactions on Automation Science and Engineering*, vol. 10, no. 3, pp. 796-806, Jul. 2013.

[52] I. Gibson, D. Rosen and B. Stucker, "*Additive Manufacturing Technologies: 3D Printing, Rapid Prototyping, and Direct Digital Manufacturing*" New York: Springer, 2015, Second Edition.

[53] J. A. Lewis and G. M. Gratson, "Direct writing in three dimensions," *Materials Today*, vol. 7, no. 7-8, pp. 32-39, Aug. 2004.

[54] L. Mortara, J. Hughes, P. S. Ramsundar, F. Livesey and D. R. Probert, "Proposed classification scheme for direct writing technologies," *Rapid Prototyping Journal*, vol. 15, no. 4, pp. 299-309, 2009.

[55] J. Niittynen, "Comparison of sintering methods and conductive adhesives for interconnections in inkjet-printed flexible electronics," Ph.D. dissertation, Tampere University of Technology, 2015.

[56] Y. Kim, B. Lee, S. Yang, I. Byun, I. Jeong and S. M. Cho, "Use of copper ink for fabricating conductive electrodes and RFID antenna tags by screen printing," *Current Applied Physics*, vol. 12, No. 2, pp. 473-478, Mar. 2012.

[57] Y. Amin, Q. Chen, L.-R. Zheng and H. Tenhunen, "Design and fabrication of wideband archimedean spiral antenna based ultra-low cost "Green" Modules for RFID Sensing and Wireless Applications," *Progress In Electromagnetics Research (PIER)*, vol. 130, pp. 241-256, 2012.

[58] K. Church et al., "Printed electronic processes for flexible hybrid circuits and antennas," *Flexible Electronics & Displays Conference and Exhibition*, pp. 1-7, Jun. 2009.

[59] P. Salonen, V. Kupiainen and M. Tuohimaa, "Direct printing of a handset antenna on a 3D surface," *IEEE International Symposium on Antennas and Propagation Society (APSURSI)*, pp. 504-505, Jan. 2013.

[60] nScrypt 3Dn series datasheet http://nscrypt.com/wp-content/uploads/2015/08/nScrypt-3Dn-Brochure.pdf (Accessed on 12th Jan 2018)

[61] E. Sipilä, J. Virkki, J. Wang, L. Sydänheimo and L. Ukkonen, "Brush-painting and photonical sintering of copper oxide and silver inks on wood and cardboard substrates to form antennas for UHF RFID tags," *International Journal of Antennas and Propagation*, vol. 2016, Article ID 3694198, 8 pages, Apr. 2016.

[62] M. Kgwadi and T. D. Drysdale, "Diode-switched thermal-transfer printed antenna on flexible substrate," *Electronics Letters*, vol. 52, no. 4, pp. 258-260, Feb. 2016.

[63] Zebra S4M Thermal Printer
https://www.zebra.com/content/dam/zebra/manuals/en-us/printer/s4m-ug-en.pdf
(Accessed on 12th Jan 2018)

[64] H. Lipson and M. Kurman, "*Fabricated: The New World of 3D Printing*" Wiley, USA, 2013.

[65] M. Mirzaee and S. Noghanian, "Additive manufacturing of a compact 3D dipole antenna using ABS thermoplastic and high temperature carbon paste," *IEEE International Symposium on Antennas and Propagation (APSURSI)*, pp. 475-476, Jun. 2016.

[66] M. Hoyack, J. Bjorgaard, E. Huber, M. Mirzaee and S. Noghanian, "Connector design for 3D printed antennas," *IEEE International Symposium on Antennas and Propagation (APSURSI)*, pp. 477-478, Jun. 2016.

[67] M. Mirzaee, S. Noghanian, L. Wiest and I. Chang, "Developing flexible 3D printed antenna using conductive ABS materials," *IEEE International Symposium on Antennas and Propagation & USNC/URSI National Radio Science Meeting*, pp. 1308-1309, Jul. 2015.

[68] K. Nate and M. M. Tentzeris, "A novel 3-D printed loop antenna using flexible NinjaFlex material for wearable and IoT applications," *IEEE Electrical Performance of Electronic Packaging and Systems (EPEPS)*, pp. 171-174, Oct. 2015.

[69] S. Moscato et al., "Infill dependent 3-D Printed material based on ninjaflex filament for antenna applications," *IEEE Antennas and Wireless Propagation Letters*, vol. 15, no. pp. 1506-1509, Jan. 2016.

[70] Prenta Duo 3D Printer
http://www.prenta.fi (Accessed on 12th Jan 2018)

[71] A. Tsolis, W. G. Whittow, A. A. Alexandridis, and J. C. Vardaxoglou, "Embroidery and related manufacturing techniques for wearable antennas: Challenges and opportunities," *Electronics*, vol. 3, pp. 314-338, May 2014.

[72] R. Rahimi, W. Yu, T. Parupudi, M. Ochoa, and B. Ziaie, "A low-cost fabrication technique for direct sewing stretchable interconnetions for wearable electronics," *International Conference on Solid State Sensors, Actuators and Microsystems (TRANSDUCERS)*, pp. 1350-1353, Jun. 2015.

[73] S. P. Pinapati, D. C. Ranasinghe and C. Fumeaux, "Characterization of conductive textiles for wearable RFID applications," *International Conference on Electromagnetics in Advanced Applications (ICEAA)*, pp. 341-344, Nov. 2016.

[74] Husqvarna Viking embroidery
http://www.husqvarnaviking.com/Machines/DESIGNER-RUBY-Royale (Accessed on 12th Jan 2018)

[75] Shieldex, 110f34 dtex 2-ply HC, High Grade Multifilament Nylon Yarn, 2014 http://www.shieldextrading.net/products/yarns-threads/ (Accessed on 12th Jan 2018)

[76] J. Niittynen, R. Abbel, M. Mäntysalo, J. Perelaer, U. S. Schubert, and D. Lupo, "Alternative sintering methods compared to conventional thermal sintering for inkjet printed silver nanoparticle ink," *Thin Solid Films*, vol. 556, pp. 452-459, Apr. 2014.

[77] Xenon Sinteron 2010-L. Installation and User Manual. Xenon Corporation, June 2013.

[78] J. Virtanen, J. Virkki, A. Z. Elsherbeni, L. Sydänheimo and L. Ukkonen, "A selective ink deposition method for the cost-performance optimization of inkjet-printed UHF RFID tag antennas," *International Journal of Antennas and Propagations*, vol. 2012, pp. 1-9, Mar. 2012.

[79] J. Virkki, J. Virtanen, L. Sydänheimo, M.M. Tentzeris, L. Ukkonen, "Embedding Inkjet-printed antennas into plywood structures for identification and sensing," *IEEE International conference on RFID Technology and Applications*, pp. 34-39, Jan. 2012.

[80] M. Akbari, et al. "Fabrication and characterization of graphene antenna for low-cost and environmentally friendly RFID tags," *IEEE Antennas Wireless Propagation Letters*, vol. 15, pp. 1569-1572, Nov. 2016.

[81] S. Enderling et al., "Sheet resistance measurement of non-standard cleanroom materials using suspended Greek cross test structures," *IEEE Transactions on Semiconductor Manufacturing*, vol. 19, no. 1, pp. 2-9, Feb. 2006.

[82] Y. Wei, Y. Li, R. Torah and J. Tudor, "Laser curing of screen and inkjet printed conductors on flexible substrates," *Symposium on Design, Test, Integration and Packaging of MEMS/MOEMS (DTIP)*, pp. 1-4, Jul. 2015.

[83] S. M. Abbas, K. P. Esselle and Y. Ranga, "A printed dual band antenna with a ground plane and electromagnetically-coupled feed for wireless body area networks," *International Workshop on Antenna Technology: Small Antennas, Novel EM Structures and Materials, and Applications (iWAT)*, pp. 15-17, Nov. 2014.

[84] M. W. A. Khan, T. Björninen, L. Sydänheimo and L. Ukkonen, "Characterization of two-turns external loop antenna with magnetic core for efficient wireless powering of cortical implants," *IEEE Antennas and Wireless Propagation Letters*, vol. 15, pp.1410-1413, Dec. 2016.

Tampereen teknillinen yliopisto
PL 527
33101 Tampere

Tampere University of Technology
P.O.B. 527
FI-33101 Tampere, Finland

ISBN 978-952-15-4181-0
ISSN 1459-2045